



Self-Aware Swarm Navigation in Autonomous Exploration Missions

Downloaded from: <https://research.chalmers.se>, 2024-04-25 12:37 UTC

Citation for the original published paper (version of record):

Zhang, S., Poehlmann, R., Wiedemann, T. et al (2020). Self-Aware Swarm Navigation in Autonomous Exploration Missions. *Proceedings of the IEEE*, 108(7): 1168-1195.
<http://dx.doi.org/10.1109/JPROC.2020.2985950>

N.B. When citing this work, cite the original published paper.

© 2020 IEEE. Personal use of this material is permitted. Permission from IEEE must be obtained for all other uses, in any current or future media, including reprinting/republishing this material for advertising or promotional purposes, or reuse of any copyrighted component of this work in other works.

Self-Aware Swarm Navigation in Autonomous Exploration Missions

This article presents methods for incorporating self-awareness into a swarm navigation system through a case study.

By SIWEI ZHANG¹, Member IEEE, ROBERT PÖHLMANN², Member IEEE,
THOMAS WIEDEMANN³, Member IEEE, ARMIN DAMMANN⁴, Member IEEE,
HENK WYMEERSCH⁵, Senior Member IEEE, AND PETER ADAM HOEHER⁶, Fellow IEEE

ABSTRACT | A multitude of autonomous robotic platforms collectively organized as a swarm attracts increasing attention for remote sensing and exploration tasks. A navigation system is essential for the swarm to collectively localize itself as well as external sources. In this article, we propose a self-aware swarm navigation system that is conscious of the causality between its position and the localization uncertainty. This knowledge allows the swarm to move in a way to not only account for external mission objectives but also enhance position information. Position information for classical navigation systems has already been studied with the Fisher information (FI) and Bayesian information (BI) theories. We show how to extend these theories to a self-aware swarm navigation system, particularly emphasizing the collective performance. In this respect, fundamental limits and geometric interpretations of localization with generic observation models are discussed. We further

propose a general concept of FI and BI based information seeking swarm control. The weighted position Cramér-Rao bound (CRB) and posterior CRB (PCRB) are employed flexibly as either a control cost function or constraints according to different mission criteria. As a result, the swarm actively adapts its position to enrich position information with different emerging collective behaviors. The proposed concept is illustrated by a case study of a swarm mission for gas exploration on Mars.

KEYWORDS | Collective intelligence; cooperative SLAM; Cramér-Rao bound (CRB); Fisher information (FI); information-seeking control; localization; multiagent systems; source localization; swarm.

I. INTRODUCTION

In nature, swarm behavior refers to grouping of numerous biological entities, for example, bird flocking, mammal herding, insect swarming, or fish schooling [1]. Each entity (or agent) follows simple interaction rules based on the observation of its surrounding [2], yet the whole swarm acts as a single organ with emerging global situation awareness and collective behaviors, such as immigrating, foraging, or escaping from predators [3], [4]. Robotic swarms, analogous to biological swarms in nature, are self-organized multiagent systems composed of a crowd of collaborative artificial entities [5]–[8]. Autonomous robotic swarm systems are suitable for sensing and exploration, for example, for search and rescue [9], environmental monitoring [10], and extraterrestrial missions [5], [11]–[13]. Humans interact with an autonomous swarm by high-level abstract mission objectives, such as search for life forms, water, mineral resources, or gas releasing sources. It is up to the swarm itself to decide on the minutiae of an efficient exploration strategy, based on its perception of the surrounding [14].

Manuscript received May 31, 2019; revised January 31, 2020 and March 24, 2020; accepted March 31, 2020. Date of publication May 7, 2020; date of current version June 18, 2020. This work was supported in part by the Helmholtz Association Project “Autonomous Robotic Networks to Help Modern Societies (ARCHES)” under Grant ZT-0033 and in part by the German Research Foundation (DFG) under Contract FI 2176/1-2 and Contract HO 2226/17-2. (Corresponding author: Siwei Zhang.)

Siwei Zhang, Robert Pöhlmann, Thomas Wiedemann, and Armin Dammann are with the Institute of Communications and Navigation, German Aerospace Center (DLR), 82234 Wessling, Germany (e-mail: siwei.zhang@dlr.de; robert.poehlmann@dlr.de; thomas.wiedemann@dlr.de; armin.dammann@dlr.de).

Henk Wymeersch is with the Department of Electrical Engineering, Chalmers University of Technology, 412 96 Gothenburg, Sweden (e-mail: henkw@chalmers.se).

Peter Adam Hoehner is with the Chair of Information and Coding Theory, University of Kiel, 24143 Kiel, Germany (e-mail: ph@tf.uni-kiel.de). This article has supplementary downloadable material available at <https://ieeexplore.ieee.org>, provided by the authors. This includes six video clips showing the evolution of the swarm formations over time steps in all six information seeking swarm control scenarios summarized in Table 3. This material is 7.3 MB in size.

Digital Object Identifier 10.1109/JPROC.2020.2985950

This work is licensed under a Creative Commons Attribution 4.0 License. For more information, see <https://creativecommons.org/licenses/by/4.0/>

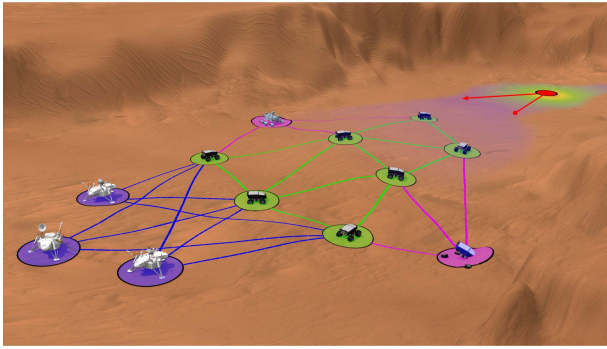


Fig. 1. Swarm system for a future Mars exploration mission: The swarm autonomously drives from the landing site to an exploration area, where a gas source may be present. Agents, landers, mobility incapacitated rovers, and a gas source are marked in green, blue, magenta, and red, respectively. The lines indicate observation links between entities, with the same color code as the emitters.

Compared to a single robot used in state-of-the-art (s.o.t.a.) exploration such as the Mars rover Curiosity [15], a swarm system offers various advantages. First, the exploration efficiency increases due to collaboration [5]. Second, the inherent system redundancy avoids single point of failures that could jeopardize the whole mission [16]. Last but not least, a spread-out swarm can be seen as a distributed sensor array with dynamically adaptable sensing area and resolution. Here, we refer to spatio-temporal processes generated from some physical phenomena as signals. Examples are luminous [8], radio frequency (RF) [17]–[20], acoustic [21], [22], gas [23], and seismic [24] emissions [8], [13]. The signals emitted either internally from the swarm or by external entities can be observed simultaneously at multiple spatial points within the sensing area of a swarm. The sensing area, referred to as the swarm's aperture [25] analogous to the antenna array's aperture in array signal processing [26], plays a decisive role in enhancing the environmental perception and situation awareness of a swarm.

An example of a swarm system for a future Mars exploration mission is illustrated in Fig. 1. A swarm of rovers, or agents (marked in green), autonomously drive from the mission base (bottom left) to an exploration area (upper right), where a gas source (marked in red) may be present. Agents observe RF signals from three landers (marked in blue), and two mobility incapacitated rovers (marked in magenta) referred to as external RF sources and other agents. Agents also measure the concentration of gas, emitted from the gas source. The swarm exploits their observations of these signals to navigate itself toward the area of interest.

Swarm navigation is composed of two interconnected research topics, namely swarm localization, where a swarm collectively estimates its own position and the positions of external sources, and swarm control, where the swarm manipulates its position to actively seek position information of itself and external sources, without losing track of other mission objectives. We are particularly

interested in a class of challenging source exploration applications. A large-scale swarm is especially favorable in these applications. The swarm extends the localizable area to enable operation outside the direct coverage of the mission base, which is crucial for the localization of distant sources. Problem formulations of swarm localization and swarm control are stated in Section II-D.

Even though extensive research has been conducted to localization and control, a study particularly emphasizing on the unique properties of the self-aware swarm navigation is still missing. We first present a brief survey on the s.o.t.a. research related to swarm localization and control, and then introduce the concept of self-aware swarm navigation addressed in this article.

A. Research Related to Swarm Localization

Localization is a classical problem in signal processing and robotics. The geometrical relationship of a group of objects is determined by, for example, distance and angle-related observations between objects. Swarm localization aims to jointly localize the swarm itself and external sources. Closely related topics are network localization, co-operative positioning [27], co-operative simultaneous localization and mapping (SLAM) [28], simultaneous localization and tracking (SLAT) [29], [30], and simultaneous localization and synchronization (SLAS) [31].

The theoretical foundations of network localizability are established by the rigidity theory [32]. Fundamental limits of localization performance are addressed with the help of mathematical tools in estimation theory. Due to its computational simplicity, Fisher information (FI) [20], [33], [34] is widely employed to assess the potentially achievable performance of non-Bayesian estimation. The Cramér–Rao bound (CRB), derived from the FI matrix (FIM), lower bounds the variance of an unbiased non-Bayesian estimator. However, due to the matrix inversion involved in the CRB calculation, it is difficult to interpret which impacts system parameters have on estimation performance. Nonmatrix-inversion expressions of the CRB have been derived, for example, in [35] and [36] to gain more insights into geometric interpretation of source localization. In [37], the CRB is derived for vehicular localization applications, indicating mutual benefits of joint self- and source localization. When combined with Bayes' theory, FI can be extended to Bayesian information (BI) [38]–[40]. The posterior CRB (PCRB) derived from the BI matrix (BIM) lower bounds the estimation root mean square error (RMSE) of a Bayesian estimator.

In practice, numerous localization algorithms have been developed [27], [41], which can be categorized by the location of estimation into centralized [42] and decentralized algorithms [27], [43]–[45]; by the extractable position-related signal features into signal power, carrier phase or symbol delay-based algorithms [17], [18], [46]; by the measurement of abstraction level into direct localization [47]–[49] and a two-stage approach [17]; by the model of unknown parameters into non-Bayesian

algorithms for deterministic parameters like least-square (LS), Gauss–Newton algorithm [46], convex-relaxation-based approaches such as semi-definite programming (SDP) [50] and alternating direction method of multipliers (ADMM) [42], or Bayesian algorithms for random variables [51] like Kalman filter (KF) [45], particle filter (PF) [52], [53], or message passing (MP) algorithms [27], [48], [54].

The choice of algorithm for swarm localization depends on the application. For system evaluation and performance benchmarking, centralized Bayesian localization algorithms like the extended KF (EKF) are preferable. For a real mission, decentralized algorithms with low-to-moderate complexity like the sum-product algorithm over a wireless network (SPAWN) [27] are favorable.

B. Research Related to Swarm Control

Swarm control is the second essential component of swarm navigation. The swarm determines on its own where to go according to certain objectives. First, from a global perspective, the swarm decides a single or a few directions to move according to mission objectives, such as approaching to an area of interest, a water or gas source, mineral resource, biological signature, etc. Second, from a swarm collective view, the swarm is manipulated into a preferable formation according to certain criteria, such as remain connected or localizable, and adapting its aperture to improve sensing tasks. Last but not least, from the view of an individual agent, certain critical objectives need to be fulfilled, such as collision avoidance, agent's position uncertainty constraints, energy considerations, and physical mobility limitations.

Multiagent control [25], [55]–[58] is a research topic closely related to swarm control and has been intensively investigated. A key focus of multiagent control is formation control. The goal is to achieve and maintain a stable formation as close as possible to a predefined target formation, or according to a target group geometry relationship. Formation control can be classified according to the available geometrical information into position-based, displacement-based, and distance-based control [55]. Another focus of multiagent control is to co-operatively accomplish abstract external goals, such as maximizing the coverage, task assignment, and path planning [25]. Other multiagent control schemes exist as well. One example is the nature-inspired flocking algorithm [59], which acts according to the three heuristic rules of swarming proposed in [2], that is, cohesion (stay close to each other), separation (avoid collisions), and alignment (match velocity).

Precise position or relative geometrical information is assumed in most of the multiagent control schemes. The uncertainty in geometrical information is often overlooked. Some formation control schemes do include this information but in a tolerance-base [60]–[62], that is, to evaluate the effectiveness of the controller with the presence of position uncertainty.

Very few studies have been conducted in controlling multiagent systems to improve the knowledge of position. In [63], formation is controlled to guarantee the rigidity of the agent network, but the impacts of measurement quality are neglected. In [64], linear state transition and measurement models are assumed, both distorted by additive white Gaussian noise (AWGN). With this simplified model, the covariance matrix obtained from a KF is exploited to achieve preferable swarm formations for both self- and source localization. In [30], a Bayesian framework is proposed, supporting only a few agents due to its high complexity. We refer to a swarm's actively foraging internal and external position information as information seeking control, which reflects the self-awareness of the swarm navigation system and thus is a focus of this article.

C. Self-Aware Swarm Navigation

Self-awareness is a concept which originated in philosophy and psychology [65], [66]. To distinguish, engineered self-awareness in man-made systems is often referred to as computational self-awareness [67]. In this article, we adapt the concept of computational self-awareness in [67], and refer to it as self-awareness for conciseness. Although self-awareness can also be analyzed for a single agent, this article deals with self-awareness emerging from the collective behavior of many agents forming a swarm. Collectivity is an essential distinguishable property of self-aware swarm navigation compared to traditional navigation systems. The massive number of measurement links in an extended swarm network is advantageous in estimating not only the positions of agents and external sources. Moreover, additional parameters of the signal model can be estimated, such as signal emission intensity, signal propagation parameters, clock, and carrier phase offsets of the emitter and the receivers. We refer to these additional parameters as nuisance parameters, which affect the observation models. The vectors of parameters (both position and nuisance parameters) related to the swarm itself and external sources are referred to as the internal and the external states, respectively. The vector of all parameters is referred to as the state of the self-aware swarm navigation system. Let us consider an extended swarm network composed of $|\mathcal{A}|$ agents in agent set \mathcal{A} and $|\mathcal{S}|$ external sources in source set \mathcal{S} . A calligraphic letter like \mathcal{P} denotes a set with cardinality $|\mathcal{P}|$ throughout this article. On the one hand, there are up to the order of $\mathcal{O}(|\mathcal{A}|^2)$ agent-to-agent (A2A) links and the order of $\mathcal{O}(|\mathcal{A}| \cdot |\mathcal{S}|)$ source-to-agent (S2A) links in the extended network. On the other hand, the dimensions of the internal and external states are in the order of $\mathcal{O}(|\mathcal{A}|)$ and $\mathcal{O}(|\mathcal{S}|)$, respectively. Therefore, for a large-scale swarm with $|\mathcal{A}| \rightarrow \infty$, the state estimation problem is in general in the order of $\mathcal{O}(|\mathcal{A}|)$ overdetermined, hence solvable. As a result, a dense swarm network is suitable for simultaneous localization and generic parameter estimation (SLAX), which is a generalization of a class of problems. The state of the

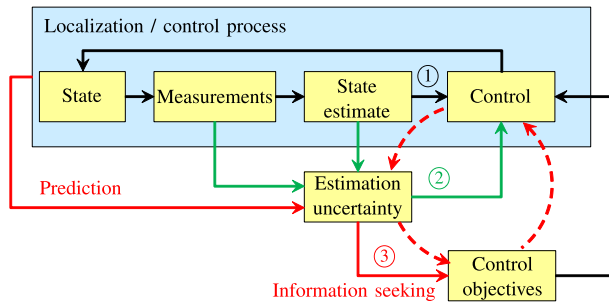


Fig. 2. Self-aware swarm navigation: The three levels of position information usage are illustrated with arrows colored in black, green, and red. These can be loosely mapped to levels of self-awareness. The red dashed arrows emphasize the swarm's self-awareness and self-expression loop, deferring from traditional navigation systems.

generalized problem can include target objects' positions as in SLAT, clock characteristics as in SLAS, and landmarks as in SLAM. For classical localization systems like the global navigation satellite system (GNSS), the number of independent observations is essential. Contrarily, for swarm localization, we can evaluate the performance at $|\mathcal{A}| \rightarrow \infty$ asymptotics, where only the swarm's aperture and the underlying observation model play essential roles. This property offers a new perspective to investigate the general geometric interpretation of swarm localization, especially when treating generic observation models with nuisance parameters.

The architecture of self-aware swarm navigation is shown in Fig. 2, where we distinguish three levels of information usage in swarm navigation. For level ①, we have a swarm localization algorithm, which estimates the state based on received signals. This localization algorithm, for example, an EKF or a PF, can optionally use historical information. Any information about estimation uncertainty, which might be provided by the localization algorithm, is not used for control. Hence, the controller uses only the "hard output" state estimates. This level of information usage corresponds to a traditional navigation system. With level ②, the estimation uncertainty provided by the localization algorithm is additionally used for control. Hence, the controller exploits "soft output" state estimates. This estimation uncertainty can be obtained by CRB, PCRb, the posterior covariance matrix from an EKF, the *a posteriori* probability density function (pdf) from a PF, or the belief from an MP algorithm. The usage of state uncertainty in control is commonly referred to as stochastic control [68]. With both level ① and level ②, the control objectives are defined outside of the control loop. The level ③ information usage is fundamentally different from the first two levels. In this level, the swarm is aware of the causality between its position and the estimation uncertainty. This knowledge allows the swarm to "look into the future," to foresee the effect of agents' movements on the estimation performance. In addition, the prediction of the estimation uncertainty is leveraged by

information seeking control. The swarm is steered toward favorable positions for localization without losing track of other mission objectives. In comparison with the first two levels, the information seeking control objective in level ③ is defined internally to the control loop, aimed at improving the swarm navigation system by itself.

Instead of classifying the system according to position information usage, a different perspective is provided by the literature on self-awareness. Systems featuring self-awareness can be classified into five levels of self-awareness [67], [69], which also have counterparts in the psychological domain [65]. In increasing order they are named stimulus-aware, interaction-aware, time-aware, goal-aware, and meta-self-aware. Level ① and level ② information usage from Fig. 2 correspond to stimulus-aware self-awareness. The system acts upon stimuli (i.e., measurements), but is not aware of consequences. Level ③ position information usage enables the system to look into the (likely) future and consider the consequences that its actions have. This adds interaction-awareness and time-awareness to the system. With that, the overall goals, that is, improving localization performance of both agents and external sources, are inherently implemented in the system design. Self-awareness can also be differentiated into private self-awareness, referring to a system's ability to acquire knowledge on internal phenomena, and public self-awareness, referring to the ability to acquire knowledge based on or about external phenomena [67]. Swarm navigation exhibits both private and public self-awareness, where self-localization of the swarm agents contributes to private and localization of external sources to public self-awareness. While self-awareness treats the acquisition of knowledge, a closely related, crucial component of a self-aware system is self-expression, which refers to the process of determining and executing actions based on this knowledge [67]. For swarm navigation, it is the control part which constitutes self-expression. The red dashed arrows in Fig. 2 emphasize the self-awareness and self-expression loop of swarm navigation.

Self-awareness decisively determines the achievable autonomy level of a swarm navigation system, thus is essential for the success of an autonomous exploration mission.

D. Contributions

The aim of this tutorial-style article is threefold: First, we present step-by-step the methodology of exploiting FI and BI to collectively analyze large-scale navigation systems. Second, we introduce the general concept of formulating the self-awareness of large-scale navigation systems with FI and BI for system self-adaptation. Third, we demonstrate the usage of the proposed concept with a case study. The main contributions of this article are as follows.

- We provide a generic swarm navigation system model, where the swarm navigates based on observed signals emitted from both internal and external

nodes. A unified radial signal model is presented with intensity-based or propagation-time-based signal features for navigation.

- We present general forms of the swarm self- and source localization CRB and PCRB, which provide theoretical limits of the localization performance. A collective view on these limits is obtained for a large-scale swarm at $|\mathcal{A}| \rightarrow \infty$ asymptotics.
- With the collective view, we derive nonmatrix-inversion expressions of the source localization CRB, which offer intuitive insights into the general impacts of aperture geometry and observation models on swarm source localization.
- We propose a general concept of information seeking swarm control, where the gradient of the predicted CRB or PCRB is exploited as control objective. This makes the swarm aware of the causality between agent positions and localization uncertainty, so it autonomously adapts itself to preferable positions for localization.
- We apply the self-aware swarm navigation concept in a case study of the Mars swarm exploration mission depicted in Fig. 1. The descriptive results complement the theoretical investigation.

E. Notation and Structure

In this section, we use a and b to denote generic (scalar or vector) variables, m and n to denote generic integers, \mathbf{a} to denote generic vectors, and \mathbf{A} and \mathbf{B} to denote generic matrices. Throughout this article, we use the following notation.

Scalars are denoted with regular letters, column vectors with lower bold letters, and matrices with capital bold letters. Capital blackboard bold letters like \mathbb{G} denote coordinate systems, except $\mathbb{R}^{m \times n}$ denoting the set of real-valued matrix with dimension $m \times n$. Lowercase blackboard bold letters denote nodes \mathfrak{o} , links \mathfrak{e} , and points \mathfrak{p} in the extended swarm network. State vectors are generally written with letter \mathbf{x} , which contains position denoted with letter \mathbf{p} and nuisance parameters denoted with letter \mathbf{a} . An estimate of variable a is indicated with \hat{a} . A variable related to a is defined with \tilde{a} to be distinguished from a . FIM of a vector \mathbf{a} is generally defined with $\mathbf{I}_{\mathbf{a}}$, distinguished from the BIM denoted as $\mathbf{J}_{\mathbf{a}}$, and the identity matrix \mathbf{I} (with nonspecific dimension) or $\mathbf{I}_{n \times n}$ (with dimension $n \times n$). Matrices (or vectors) with all entries being zero are denoted as $\mathbf{0}$ (with nonspecific dimension) or $\mathbf{0}_{m \times n}$ (with dimension $m \times n$). Similarly, matrices (or vectors) with all entries being one are denoted as $\mathbf{1}$ or $\mathbf{1}_{m \times n}$. Symbol \otimes denotes the Kronecker product. Operators $\text{tr}[\cdot]$ and $\det[\cdot]$ are trace and determinant of a matrix. Operators $\text{vec}\{\cdot\}$ and $\text{diag}\{\cdot\}$ arrange elements (scalars or vectors) into a vector and a diagonal matrix, respectively. Braces $\{\cdot\}$ denotes a set of elements. Operator $\|\cdot\|$ represents the Euclidean norm. Notation $\mathbf{A} \succcurlyeq \mathbf{B}$ indicates that matrix $\mathbf{A} - \mathbf{B}$ is positive-semidefinite. Notation $p(a; b)$ and $p(a|b)$ denote the pdf of a given deterministic and random variable b , respectively.

Operators $\mathbb{E}_a[\cdot]$ and $\text{cov}_a[\cdot]$ denote expectation and covariance over $p(a)$. We use superscripts in parentheses to denote variables at specific time step n as (n) , from step m to step n as $(m : n)$, at a nonspecific previous and current time step as $(-)$ and $(+)$, from step n to nonspecific previous and current time as $(n : -)$ and $(n : +)$. The notation $\mathbf{A}_{(m,n)}$ denotes the entity at the m th row and n th column of a generic matrix \mathbf{A} . The notation $\mathbf{A}_{\langle \mathbf{a}, \mathbf{b} \rangle}$ denotes a submatrix of \mathbf{A} , truncated at the rows and columns corresponding to the state \mathbf{a} and \mathbf{b} , respectively.

The rest of this article is organized as follows. The generic swarm navigation system model is introduced in Section II. Theoretical limits and geometric interpretation on swarm localization is discussed in Section III. In Section IV, information seeking swarm control is introduced. In Section V, we present a case study of the self-aware swarm navigation system in the Mars exploration mission. We provide a discussion on the potential extensions of the proposed self-aware swarm navigation concept in Section VI, and draw our conclusion in Section VII.

II. SWARM NAVIGATION SYSTEM MODEL

A. Extended Swarm Network

In this article, we consider an extended swarm network in 2-D space, for example, the swarm navigation system in the Mars exploration mission introduced in Fig. 1. A generic node \mathfrak{o}_u with index u in the network located at point \mathfrak{p}_u is either a beacon within the beacon set \mathcal{B} , an external source within the source set \mathcal{S} , or an agent within the agent set \mathcal{A} . The complete node set is denoted as $\mathcal{V} = \mathcal{B} \cup \mathcal{S} \cup \mathcal{A}$. Throughout this article, the index u preferably indicates either an agent which receives a signal, or a generic node. The index v preferably indicates a node which transmits a signal. We assume there is a sufficient number of beacons to span a unique global coordinate system \mathbb{G} , which serves as the default coordinate system of the application. The node coordinates are denoted as $\mathbf{p}_u^{\mathbb{G}} = \text{vec}\{x_u, y_u\}$. When the distance and angular information between the source and the swarm are investigated individually, for example, in source localization, a swarm polar coordinate system \mathbb{P} with the origin at the swarm center is preferable for analysis. In that case, the coordinates of the node \mathfrak{o}_u are denoted as $\mathbf{p}_u^{\mathbb{P}} = \text{vec}\{d_u, \theta_u\}$. If the coordinate system under investigation is previously specified, the superscript is often omitted for simplicity, i.e., the coordinates of node \mathfrak{o}_u are denoted as \mathbf{p}_u . The state vector of \mathfrak{o}_u is denoted as $\mathbf{x}_u = \text{vec}\{\mathbf{p}_u, \mathbf{a}_u\}$, including its coordinates \mathbf{p}_u and nuisance parameters \mathbf{a}_u . These nuisance parameters determine the observation models, for example, clock offset, carrier phase offset, or signal propagation parameters. They may be jointly estimated with the coordinates of the node. The three types of nodes, that is, beacons, sources, and agents, are distinguished as follows.

1) *Beacon*: A beacon $\phi_u \in \mathcal{B}$ is a node with perfectly known global coordinates and nuisance parameters. Beacons are synchronized static infrastructures, for example, fixed RF transmitters at the mission base. A beacon ϕ_u continuously emits a signal $s_u(t)$, which is exploited by the swarm for localization in the global coordinate system. In the context of co-operative and network localization, a beacon is also referred to as an anchor in the literature (see [27]).

2) *Source*: A source $\phi_u \in \mathcal{S}$ is an external node whose state \mathbf{x}_u is unknown and of interest to the swarm. As in the swarm exploration example introduced in Fig. 1, a source can either be a static unit emitting RF signals, which are observed by the swarm as signals of opportunity, or an environmental point source that shall be localized by the swarm, for example, a gas diffusion source. For this example, the set of sources \mathcal{S} can be further divided into the set of RF sources \mathcal{S}_{RF} and a set of gas sources \mathcal{S}_{gas} . Similar to beacons, the emitted signal from a source ϕ_u is generically denoted as $s_u(t)$. The states of all sources are represented as $\mathbf{x}_S = \text{vec}\{\mathbf{x}_u : \forall \phi_u \in \mathcal{S}\}$.

3) *Agent*: Actively controlled agents are the core components of a swarm. An agent $\phi_u \in \mathcal{A}$ emits a signal $s_u(t)$ and receives the signals $r_{uv}(t)$ emitted from node $\phi_v \in \mathcal{V}$ through unidirectional links ϕ_{uv} . Measurements \mathbf{z}_{uv} can be obtained from $r_{uv}(t)$, extracting the geometric relationship between ϕ_u and ϕ_v contained in the signal features \mathbf{g}_{uv} . All links in the extended swarm network are included in the total link set \mathcal{E} , and can be classified according to the origin of the signal as beacon-to-agent (B2A), S2A, and A2A links. Depending on the type of signal, a limited effective measurement coverage may be applied, which defines the maximum distance between the origin and an agent, such that the observed signal can effectively be exploited for localization. The swarm collects measurements $\mathbf{z} = \text{vec}\{\mathbf{z}_{uv} : \forall \phi_{uv} \in \mathcal{E}\}$ from all links to jointly estimate the internal state \mathbf{x}_A and the external state \mathbf{x}_S . The total state to be estimated is $\mathbf{x} = \text{vec}\{\mathbf{x}_A, \mathbf{x}_S\}$. The nodes with unknown parameters are included in the set $\mathcal{X} = \mathcal{A} \cup \mathcal{S}$.





While the explicit assignment of nodes to different sets is fixed, nodes can nevertheless take different implicit roles during a mission. An agent who is not moving for a while can accumulate precise absolute position information and can thus act as a quasi-beacon to other agents. Vice versa, an agent outside of the swarm or a remote beacon can be considered as a source to the swarm, when relative positions of nodes are of interest.

Types of nodes considered in the extended swarm network are summarized in Table 1. In this article, red markers denote either generic sources or specifically gas sources.

B. Dynamic Model

Having defined the entities and sets in the extended swarm network, we have a look at the dynamic model of agents. In many applications, the temporal evolution of

Table 1 Nodes in an Extended Swarm Network

Name (set)	Node ($\phi_u \in \mathcal{V}$)			
	Beacon (\mathcal{B})	Node with unknowns (\mathcal{X})		
		Agent (\mathcal{A})	Source (\mathcal{S})	
			RF (\mathcal{S}_{RF})	Gas (\mathcal{S}_{gas})
Symbol				
State (remark)	\mathbf{x}_B (known)	\mathbf{x}		
		\mathbf{x}_A		\mathbf{x}_S
		\mathbf{p}_A (controllable)	\mathbf{a}_A	$\mathbf{x}_{S_{\text{RF}}}$ $\mathbf{x}_{S_{\text{gas}}}$
		(to be estimated)		

the network state is of interest, instead of a snapshot of the current state. One example is Bayesian tracking, where temporal coherency of the state is exploited to improve the current state estimation. Another example is swarm control, where a control command is applied to the swarm for spatial transition. Bayes' theorem is often applied to estimation problems with dynamics, or more general, with *a priori* information. A Bayesian estimator treats states $\mathbf{x}^{(+)}$ as random variables and estimates them from the *a posteriori* pdf $p(\mathbf{x}^{(+)}|\mathbf{z}^{(+)})$, which incorporates the *a priori* pdf $p(\mathbf{x}^{(+)})$ and the observation likelihood function $p(\mathbf{z}^{(+)}|\mathbf{x}^{(+)})$ by Bayes' rule

$$p(\mathbf{x}^{(+)}|\mathbf{z}^{(+)}) \propto p(\mathbf{z}^{(+)}|\mathbf{x}^{(+)})p(\mathbf{x}^{(+)}). \quad (1)$$

With a state transition model and the first-order Markov assumption, the Bayesian estimation framework can be extended to a recursive expression of the *a posteriori* filtered density $p(\mathbf{x}^{(+)}|\mathbf{z}^{(1:+)})$ with sequential measurements as

$$p(\mathbf{x}^{(+)}|\mathbf{z}^{(1:+)}) \propto p(\mathbf{z}^{(+)}|\mathbf{x}^{(+)}) \int p(\mathbf{x}^{(+)}|\mathbf{x}^{(-)})p(\mathbf{x}^{(-)}|\mathbf{z}^{(1:-)})d\mathbf{x}^{(-)}. \quad (2)$$

Equation (2) is the foundation of recursive Bayesian tracking algorithms such as different variants of KFs and PFs. The derivation of (2) is well known and can be found for example in [52] and [70]. Once the *a posteriori* filtered density $p(\mathbf{x}^{(+)}|\mathbf{z}^{(1:+)})$ is acquired, a point estimate of the state $\hat{\mathbf{x}}^{(+)}$ can be obtained in a minimum mean square error (MMSE) or maximum *a posteriori* (MAP) manner.

Agents collaborate in the sense of actively adapting their positions so that the emerging swarm formation is optimized according to certain mission objectives. In our example, these objectives includes minimizing the position uncertainty of the swarm and external sources, that is, information seeking, approaching to an area of interest, and avoiding collision. In this article, we mainly consider measurements that provide geometric information

between nodes. The dynamic parameters of an agent, such as velocity, acceleration, and heading, are not included in the state. An extension to the dynamic state space is straightforward, as shown in [71]. The transition of the agent's position between two consecutive time steps is described by a movement model

$$\mathbf{p}_u^{(+)} = f(\mathbf{p}_u^{(-)}, \mathbf{b}_u) + \boldsymbol{\omega}_u \quad \forall \mathbf{p}_u \in \mathcal{A} \quad (3)$$

where $\mathbf{b}_u \in \mathcal{U}$ is the control command of agent \mathbf{p}_u within a feasible control set \mathcal{U} , and $\boldsymbol{\omega}_u$ is additive state transition noise. Parameters other than agents' positions are assumed to be static. These parameters include the nuisance parameters of an arbitrary node and the positions of nonagent nodes. We combine the control commands of all agents to $\mathbf{b}_\mathcal{A} = \text{vec}\{\mathbf{b}_u : \forall \mathbf{p}_u \in \mathcal{A}\}$, and denote the collective feasible control set as $\mathcal{U}_\mathcal{A}$. Variants of objective functions can be defined according to the employed signal processing models, for example, the Bayesian and non-Bayesian models, which will be discussed in detail in Section IV.

C. Signals and Observations in a Swarm

Different types of physical emission processes can be modeled with partial differential equations (PDEs), such as the wave equation for RF, seismic and acoustic waves, or the diffusion equation for gas and heat diffusion. If the emission area of the physical process is small enough, it can be approximated as a point emitter, such as an external source, a beacon, or another agent. We only focus on the isotropic point emitter case. The distance information between the observing agent and the emitter can be extracted from intensity-based signal features like the received amplitude of RF signals [72], or the concentration of gas signals [73]. Alternatively, the distance can be estimated from the propagation time based signal features like carrier phase [26], [74], [75] and symbol delay [18], [76]–[78] of RF signals. We unify different signal observations by introducing a general signal model for signal fields generated by point sources in Section II-C1. Specific observation models for RF signals, which are the primarily used observations within this article, are discussed in detail in Sections II-C2 and II-C3. As a second special case, we derive an observation model for gas diffusion from the diffusion equation in Section II-C4.

1) *Generic Signal Model*: The solution of the spatial-temporal process PDE is normally a function of position and time. We refer to this function as the signal model. For the general case, we assume that node $\mathbf{p}_v \in \mathcal{V}$ is emitting a continuous signal $s_v(t)$. An agent $\mathbf{p}_u \in \mathcal{A}$ observes this signal through link \mathbf{p}_{uv} as

$$r_{uv}(t) = s_{uv}(\mathbf{x}_{uv}, t) + \epsilon_{uv}(t), \quad 0 \leq t < T_o. \quad (4)$$

The signal model $s_{uv}(\mathbf{x}_{uv}, t)$ contains the emitted signal, propagation effects, as well as position-related

information about nodes \mathbf{p}_u and \mathbf{p}_v , where $\mathbf{x}_{uv} \triangleq \text{vec}\{\mathbf{x}_u, \mathbf{x}_v\}$. As (4) is general, $s_{uv}(\mathbf{x}_{uv}, t)$ can be either real- or complex-valued, depending on the underlying physics. For real-valued $s_{uv}(\mathbf{x}, t)$, the additive noise $\epsilon_{uv}(t)$ is a white process [79] with a power spectral density (PSD) of $N_{0,uv}/2$. In the complex-valued case, we have $\epsilon_{uv}(t) = \Re[\epsilon_{uv}(t)] + j\Im[\epsilon_{uv}(t)]$ with the real part $\Re[\cdot]$ and the imaginary part $\Im[\cdot]$ being white processes with a PSD of $N_{0,uv}/2$. The letter j denotes the imaginary unit. As $\epsilon_{uv}(t)$ is zero-mean, $s_{uv}(\mathbf{x}_{uv}, t)$ represents the mean of $r_{uv}(t)$.

Particularly for signals sent out from point emitters that radially propagate into the environment, the signal fronts are spherical. Hence, the received signal depends only on the emitter-to-receiver distance and time. Therefore, the geometric relationship of the emitter and receiver is solely embedded in distance-related signal features.

The signal features $\mathbf{g}_{uv} = \mathbf{g}(d_{uv}, \mathbf{a}_u, \mathbf{a}_v)$ are expressed as real-valued functions of real-valued nuisance parameters $\mathbf{a}_u, \mathbf{a}_v$ and distance d_{uv} . Both signal feature functions and nuisance parameters are determined by the underlying physical models.

2) *Generic RF Signals*: RF propagation from an emitter \mathbf{p}_v to a generic point \mathbf{p}_u over a distance d_{uv} is described by the spherical wave equation

$$\frac{\partial^2 d_{uv} E(\mathbf{p}_u, t)}{\partial d_{uv}^2} = \frac{1}{c^2} \frac{\partial^2 d_{uv} E(\mathbf{p}_u, t)}{\partial t^2} \quad (5)$$

with the speed of light c , electric field $E(\mathbf{p}_u, t)$, and time t , which can be derived from the Maxwell equations [26, p. 465]. Equation (5) holds for electric fields $E(\mathbf{p}_u, t)$, when the medium of propagation is homogeneous and nondispersive. The generic solution to (5) is of the form

$$E(\mathbf{p}_u, t) = \frac{1}{d_{uv}} s_+(t - d_{uv}/c) + \frac{1}{d_{uv}} s_-(t + d_{uv}/c) \quad (6)$$

where $s_+(t)$ and $s_-(t)$ are two arbitrary functions. We are only interested in the outward traveling wave $1/d_{uv} s_+(t - d_{uv}/c)$, that is, the signal traveling from the emitter into the environment. Particularly, for an RF point emitter \mathbf{p}_v , the outward traveling wave can be modeled as

$$d_{uv}^{-1} s_+(t - d_{uv}/c) = d_{uv}^{-1} A_v e^{j\omega_v(t - d_{uv}/c)} s_v(t - d_{uv}/c) \quad (7)$$

with the transmit power A_v^2 and the normalized transmitted baseband signal $s_v(t)$ modulated onto a carrier $e^{j\omega_v t}$ with carrier frequency f_v and $\omega_v = 2\pi f_v$. A receiver \mathbf{p}_u at \mathbf{p}_u would observe the down-converted and low-pass filtered baseband signal (multiplication by $e^{-j\omega_v t}$) within the observation interval $0 < t < T_o$, modeled as

$$s_{uv}(\mathbf{x}_{uv}, t) = \alpha_{uv} s_v(t - \underbrace{(d_{uv} - \delta_{uv})}_{T_{uv}}/c) \quad (8)$$

where the complex amplitude α_{uv} is expressed as

$$\alpha_{uv} = \overbrace{A_{uv} d_{uv}^{-1}}^{A_{uv}} e^{-j\omega_s(d_{uv} - \delta_{uv} - \phi_{uv})/c}. \quad (9)$$

As oscillators in transmitter and receiver are not synchronized, we have a clock offset $\delta_{uv} = \delta_u - \delta_v$ in addition to the propagation time, with δ_v and δ_u denoting the clock offsets of the transmitter and receiver with respect to (w.r.t.) a system clock, respectively. Additional phase offsets $\phi_{uv} = \phi_u - \phi_v$ can be present, for example, due to the phase-locked loops (PLLs) in the transceiver chain. The phase offsets of the transmitter and receiver w.r.t. a system phase are denoted as ϕ_v and ϕ_u , respectively. Since we are interested in the geometric information contained in the signal, both symbol delay T_{uv} and carrier phase Φ_{uv} are in units of meters. For simplicity, we assume that the carrier frequency offset and clock drift have already been compensated [80].

It can be observed that the position information can be extracted generally from the signal features like received signal magnitude A_{uv} , symbol delay T_{uv} and carrier phase Φ_{uv} , which are functions of distance between transceivers d_{uv} and nuisance parameters, that is, A_v , δ_{uv} , and ϕ_{uv} . If these nuisance parameters are known, direct range measurements can be obtained, for example, by received signal strength (RSS) from magnitude A_{uv} or time of arrival (ToA) from symbol delay T_{uv} . Ranging directly from the carrier phase is difficult due to short wavelength. However, with appropriate infrastructure and initialization, ranging with the carrier phase is possible, similar to the real-time kinematic (RTK) service in GNSS. If both forward and backward links are available, the symbol delays from both directions can be combined to the round trip time (RTT) observation. The clock offsets δ_{uv} and δ_{vu} cancel each other out, so that an equivalent direct ranging can be obtained. In the case of general unknown nuisance parameters, measurements at spatially separated points are collected by agents. Essentially, distance differences between transceivers are exploited for joint localization and parameter estimation. Concerning magnitude and symbol delay, differential RSS (DRSS) and time difference of arrival (TDoA) are utilized for localization, respectively. Regarding the carrier phase, traditional angle of arrival (AoA) measurements from the phase difference of arrival (PDoA) observations with planar signal model contain only the angular information between nodes. The curvature of arrival (CoA) measurement adopts the radial signal model, which includes both distance and angular information [36].

3) *Application Specific RF Signals*: Two types of RF signals are employed by the swarm. The first one has a higher carrier frequency f_c with $\omega_c = 2\pi f_c$, and a larger bandwidth B_c , aiming at short distance communications and intra-swarm measurements, that is, on A2A links. The second one has a much lower carrier frequency f_s with

$\omega_s = 2\pi f_s$, and a smaller bandwidth B_s , which is suitable for long distance communications and beacon or RF source to swarm measurements, that is, on B2A and S2A links. For the three different RF link classes, namely A2A, B2A, and S2A links, we consider three specific types of signal models derived from (8).

a) *Agent to agent link*: For a specific A2A link \mathbb{C}_{uv} , the signal transmitted by \mathbb{C}_v and received and downconverted to baseband by agent \mathbb{C}_u can be modeled as

$$s_{uv}(\mathbf{x}_{uv}, t) = \alpha_{uv} s_v(t - (d_{uv} - \delta_u + \delta_v)/c) \quad (10)$$

where α_{uv} is the unknown complex signal amplitude, considered as a nuisance parameter. For A2A links, the position information can be extracted from the symbol delay. Particularly, if the A2A links are always symmetric, the clock offsets from both links cancel out. In this case, A2A distance can be directly estimated from the RTT observations.

b) *Beacon to agent link*: The second type are the B2A links. Signals are emitted by beacons near the mission base. The lower carrier frequency $f_s \ll f_c$ is suitable for guiding the swarm within a wider area. Beacons' clock offsets δ_v and phase offsets ϕ_v are set to zero and assumed to be known. Due to the lower carrier frequency, we assume that in this case the position information contained in the carrier phase can be exploited in addition to the symbol delay. In order to extract geometric information from the phase, it is essential to assume that the phase offset from the agent's receiving front-end is coherent to its clock offset, that is, the phase offset of the receiver fulfills $\phi_u = \delta_u$. This assumption is valid for a direct RF sampling, as implemented in a long wavelength array (LWA) [81] or a low frequency array (LOFAR) [82] system. In the end, the phase offset in the transceiver chain becomes $\phi_{uv} = \delta_u$. A signal transmitted by beacon \mathbb{C}_v and received by agent \mathbb{C}_u is modeled in baseband as

$$s_{uv}(\mathbf{x}_{uv}, t) = A_{uv} e^{-j\omega_s(d_{uv} - \delta_u)/c} s_v(t - (d_{uv} - \delta_u)/c). \quad (11)$$

For a sufficient number of beacons, the positions of agents in the global coordinate system \mathbb{G} can be estimated from symbol delays with the TDoA observations. In addition, by exploiting the carrier phase, the AoA or CoA measurements can be utilized for agent position estimation. In the case of an insufficient number of beacons, the position of agents in \mathbb{G} is not observable. However, if the relative positions of the agents w.r.t. a swarm coordinate system are known, the beacons' positions w.r.t. the swarm coordinate system can be estimated reversely with range difference, AoA or CoA measurements. In this case, the beacons are similar to an external RF source. One application of this technique is returning to mission base [83].

c) *RF source to agent link*: The third link type under consideration are S2A links, where signals are emitted

from external RF sources. Similar to B2A signals, the RF signals on S2A links have a low carrier frequency $f_s \ll f_c$. We also assume that the carrier phase of the receiver is aligned with its clock, that is, $\phi_u = \delta_u$. A signal transmitted by source \mathfrak{Q}_v and received by agent \mathfrak{Q}_u is modeled by

$$s_{uv}(\mathbf{x}_{uv}, t) = A_{uv} e^{-j\omega_s(d_{uv} - \delta_u + \phi_v)/c} \times s_v(t - (d_{uv} - \delta_u + \delta_v)/c). \quad (12)$$

In contrast to beacons, the clocks of the RF sources are not synchronized to the system. Therefore, the unknown clock offset δ_v and phase offset ϕ_v have to be estimated jointly as nuisance parameters. Similarly, symbol delay and carrier phase can be exploited with range difference, AoA or CoA measurements for source localization.

4) *Gas Diffusion*: Gas diffusion processes can be described by PDEs, referred to as diffusion equations [84]. The gas concentration can be observed by a swarm and utilized for gas source localization. In [73], sophisticated gas diffusion models have been investigated. In this article, we consider a gas source $\mathfrak{Q}_v \in \mathcal{S}_{\text{gas}}$ at point \mathfrak{p}_v with radial diffusion to point \mathfrak{p}_u . Planar isotropic diffusion in the steady state is assumed, which approximates the diffusion of material with a density heavier than the surrounding atmosphere. With this model, similar as described in [84, p. 69], the diffusion equation simplifies to an ordinary differential equation (ODE), which depends only on the distance to the source d_{uv} , and can be expressed as

$$-\kappa \left(\frac{\partial^2 C_{uv}}{\partial d_{uv}^2} + \frac{1}{d_{uv}} \frac{\partial C_{uv}}{\partial d_{uv}} \right) = h_s(d_{uv}), \quad d_{uv} > 0 \quad (13)$$

where κ is the diffusion coefficient with unit m^2/s , C_{uv} is the gas concentration, with a unit like parts-per-billion (ppb) depending on the applications, and $h_s(d_{uv})$ is a source function. We define the source function as $h_s(d_{uv}) = \eta \cdot (1 - \sigma_H(d_{uv}/R_0 - 1))$ with σ_H indicating the Heaviside step function. The source function describes a disk with a significantly small radius, for example, $R_0 = 1$ m, which can be considered as a point in the ground, with an emission rate η with a unit of, for example, ppb/s . As a boundary condition, we assume that the concentration value reaches 0 at a distance d_{\max} from the source. In addition, we consider $(\partial C_{uv}/\partial d_{uv})|_{d_{uv}=0} = 0$. The solution of the ODE in (13) is expressed as

$$C_{uv} = \begin{cases} \frac{\eta}{2\kappa} \left(\frac{R_0^2 - d_{uv}^2}{2} + R_0^2 \ln \frac{d_{\max}}{R_0} \right), & 0 < d_{uv} \leq R_0 \\ \frac{\eta R_0^2}{2\kappa} \ln \frac{d_{\max}}{d_{uv}}, & R_0 < d_{uv} < d_{\max}. \end{cases} \quad (14a)$$

$$(14b)$$

We are interested in the second case $R_0 < d_{uv} < d_{\max}$, that is, the concentration outside the source. We can rewrite the concentration from the gas source $\mathfrak{Q}_v \in \mathcal{S}_{\text{gas}}$ at agent $\mathfrak{Q}_u \in \mathcal{A}$ within an observation window $0 < t < T_o$ as

$$s_{uv}(\mathbf{x}_{uv}, t) = C_{uv} = \ln \left(\overbrace{d_{\max}^{\frac{a_g}{2\kappa}}}^{a_g} \overbrace{d_{uv}^{-\frac{b_g}{2\kappa}}}^{b_g} \right) = C(a_g d_{uv}^{b_g}). \quad (15)$$

The signal feature considered for a gas diffusion process is the gas concentration C_{uv} . The term $C(a_g d_{uv}^{b_g})$ in (15) emphasizes that the gas concentration has two nuisance parameters, namely the scaling parameter a_g and the exponent parameter b_g , employed to the distance. The gas concentration measures the intensity of the received signal, similar to the magnitude observation of an RF source expressed in (9). With the gas source model under consideration, we assume either there is only one gas source, or there exist multiple separable sources, for example, with different types of gas. This assumption circumvents the necessity to distinguish between the received concentrations of different emission sources in the diffusion process.

The signal features in the considered extended swarm network are summarized in Table 2. We can observe that the intensity based signal features can be formulated with the distance and the scaling and exponent nuisance parameters, whereas the propagation time based signal features can be formulated as functions of distance with offsets.

D. Swarm Navigation Problem Formulation

After introducing the network and observation models, we can formulate the two problems of swarm navigation mentioned in Section I, namely swarm localization and swarm control, as follows.

1) *Swarm Localization*: The objective of swarm localization is to find an estimate $\hat{\mathbf{x}}_{\text{opt}}^{(+)}$ of the state $\mathbf{x}^{(+)}$, given measurements. Estimation quality is assessed by an error metric like the mean square error (MSE), denoted as $\text{tr}[\text{cov}[\hat{\mathbf{x}}^{(+)}]]$. A unified problem statement of swarm localization can be formulated as

$$\hat{\mathbf{x}}_{\text{opt}}^{(+)} = \arg \min_{\hat{\mathbf{x}}^{(+)}} \text{tr}[\text{cov}[\hat{\mathbf{x}}^{(+)}]]. \quad (16)$$

For non-Bayesian algorithms, only the current measurements $\mathbf{z}^{(+)}$ are considered. The error metric is specified as $\text{tr}[\text{cov}_{\mathbf{z}^{(+)}}[\hat{\mathbf{x}}^{(+)}]]$. Bayesian algorithms exploit a sequence of measurements over time $\mathbf{z}^{(1:+)}$ and the error metric of $\text{tr}[\text{cov}_{\mathbf{x}^{(+)}}[\hat{\mathbf{x}}^{(+)}]]$. For simplicity of notation, we may omit the superscript (+) in non-Bayesian localization, when there is no risk of ambiguity. In this article, we focus on the theoretical limits and geometrical interpretations of swarm localization, which is discussed in Section III.

Table 2 Distance-Related Signal Features in an Extended Swarm Network

Signal model $s_{uv}(\mathbf{x}_{uv}, t)$		RF			Gas
		B2A	S2A	A2A	
Intensity	Magnitude A_{uv}	$A(A_v^{-1}d_{uv})$	$A(A_v^{-1}d_{uv})$	$A(A_v^{-1}d_{uv})$	—
	Concentration C_{uv}	—	—	—	$C(a_g d_{uv}^{b_g})$
Propagation time	Carrier phase Φ_{uv}	$\Phi(d_{uv} - \delta_u)$	$\Phi(d_{uv} - \delta_u + \delta_v)$	—	—
	Symbol delay T_{uv}	$T(d_{uv} - \delta_u)$	$T(d_{uv} - \delta_u + \delta_v)$	$T(d_{uv} - \delta_u + \delta_v)$	—

2) *Swarm Control*: After estimating the state $\mathbf{x}^{(-1)}$ and previous to moving and acquiring the measurements $\mathbf{z}^{(+)}$, the swarm needs to decide where to go next. A control command $\mathbf{b}_A \in \mathcal{U}_A$ is generated based on the previous state estimate $\hat{\mathbf{x}}^{(-1)}$ and the predicted measurements $\hat{\mathbf{z}}^{(+)}$, and is optimized in the sense of multiobjective control criteria. The control objectives can include an information seeking cost function $f_p(\mathbf{b}_A)$, information seeking constraints $h_{p,l}(\mathbf{b}_A), l = 1, \dots, L_p$, another general mission cost function $f_m(\mathbf{b}_A)$ like goal approaching, and other general mission constraints $\mathbf{h}_m(\mathbf{b}_A)$ like collision avoidance. The overall swarm control problem can be formulated as

$$\min_{\mathbf{b}_A \in \mathcal{U}_A} \left\{ \underbrace{f_p(\mathbf{b}_A)}_{\text{(information seeking)}}, \underbrace{f_m(\mathbf{b}_A)}_{\text{(mission cost function)}} \right\} \quad (17a)$$

s.t. information seeking constraints:

$$h_{p,l}(\mathbf{b}_A) \geq 0, \quad l = 1, \dots, L_p \quad (17b)$$

mission constraints:

$$\mathbf{h}_m(\mathbf{b}_A) \geq \mathbf{0}. \quad (17c)$$

Similar to swarm localization, the information seeking objectives can be realized with both non-Bayesian (FI seeking) and Bayesian (BI seeking) assumptions. The predicted estimation covariance matrix under non-Bayesian and Bayesian assumptions, denoted as $[\text{cov}_{\hat{\mathbf{z}}^{(+)}}[\hat{\mathbf{x}}^{(+)}]]$ and $[\text{cov}_{\mathbf{x}^{(+)}}[\mathbf{z}^{(+)}, \hat{\mathbf{z}}^{(+)}][\hat{\mathbf{x}}^{(+)}]]$, are exploited for both information seeking cost function $f_p(\mathbf{b}_A)$ and constraints $h_{p,l}(\mathbf{b}_A)$. These covariance matrices are modeled with the CRB and PCRB, which are functions of \mathbf{b}_A . In addition, diagonal weighing matrices $\mathbf{\Lambda}$ and $\mathbf{\Lambda}_l$ are introduced to adapt the focus of information seeking control according to applications. The specification of the objectives is detailed in Section IV. In this article, we focus on the potential of exploiting FI and BI for swarm control. Therefore, a centralized controller design is introduced in Section IV. Decentralization of swarm navigation is discussed as an outlook in Section VI.

III. THEORETICAL LIMITS ON SWARM LOCALIZATION

A. Extractable State Information in a Swarm

Now, we that for all links $e_{uv} \in \mathcal{E}$ within the extended swarm network, a total of $|\mathcal{E}|$ signals $r_{uv}(t)$ with the generic model (4) are received. The information contained

in all these signals regarding the total state vector \mathbf{x} can be quantified by the FIM

$$\begin{aligned} \mathbf{I}_x &= \Re \left\{ \sum_{e_{uv} \in \mathcal{E}} \frac{2}{N_{0,uv}} \int_0^{T_o} \nabla_{\mathbf{x}} s_{uv}^*(\mathbf{x}_{uv}, t) \nabla_{\mathbf{x}^T} s_{uv}(\mathbf{x}_{uv}, t) dt \right\} \\ &= \sum_{e_{uv} \in \mathcal{E}} \nabla_{\mathbf{x}} \mathbf{g}_{uv}^T \mathbf{I}_{g_{uv}} \nabla_{\mathbf{x}^T} \mathbf{g}_{uv} \end{aligned} \quad (18)$$

where $\mathbf{I}_{g_{uv}}$ is the information intensity of the signal features \mathbf{g}_{uv} from the received signal $r_{uv}(t)$ [85], [86] expressed as

$$\mathbf{I}_{g_{uv}} \triangleq \frac{2}{N_{0,uv}} \int_0^{T_o} \nabla_{\mathbf{g}_{uv}} s_{uv}^*(t) \nabla_{\mathbf{g}_{uv}^T} s_{uv}(t) dt. \quad (19)$$

For a 1-D signal feature g_{uv} , the information intensity is denoted as $\iota_{g_{uv}}$. Especially, if the transformed variable is distance, $\iota_{g_{uv}}$ is referred to as ranging information intensity (RII) [87]. Following the definition in Section II-C1, (18) is valid for both real- and complex-valued $s_{uv}(t)$. For a gas source, the signal feature is the concentration defined in Section II-C4, that is, $g_{uv} = C(a_g d_{uv}^{b_g})$. The information intensity $\iota_{g_{uv}}$ is $2/N_{0,uv}$, that is, it only depends on the noise PSD. For an RF source, the distance information is embedded in the signal features amplitude A_{uv} , phase Φ_{uv} and symbol delay T_{uv} , i.e., $\mathbf{g}_{uv} = \text{vec}\{A_{uv}, \Phi_{uv}, T_{uv}\}$. Assuming that $s_{uv}(\mathbf{x}_{uv}, t)$ is modulated onto a carrier with frequency $f_v = \omega_v/2\pi$ and has a symmetric PSD, the information intensity $\mathbf{I}_{g_{uv}}$ can be expressed as

$$\mathbf{I}_{g_{uv}} = \frac{2 E_{uv}}{N_{0,uv}} \begin{pmatrix} A_{uv}^{-2} & 0 & 0 \\ 0 & \omega_v^2/c^2 & 0 \\ 0 & 0 & \beta_v^2/c^2 \end{pmatrix} \quad (20)$$

where E_{uv} and β_v^2 are the received power and the mean-square bandwidth [33] of the signal represented in frequency domain $S_v(f)$, calculated by Parseval's identity as

$$\begin{aligned} E_{uv} &\triangleq A_{uv}^2 \int_{-\infty}^{\infty} \|S_v(f)\|^2 df, \\ \beta_v^2 &\triangleq \frac{A_{uv}^2 \int_{-\infty}^{\infty} 4\pi^2 f^2 \|S_v(f)\|^2 df}{E_{uv}}. \end{aligned} \quad (21)$$

The diagonal property of (20) indicates that the position information contained in magnitude, phase, and symbol

delay can be evaluated independently. Under regularity conditions, the covariance of any unbiased estimation $\hat{\mathbf{x}}$ is lower bounded by the CRB [33], which is obtained by inverting the FIM

$$\text{cov}_{\mathbf{z}}[\hat{\mathbf{x}}] \succcurlyeq \text{CRB}[\mathbf{x}] \triangleq \mathbf{I}_{\mathbf{x}}^{-1}. \quad (22)$$

Sometimes, we are interested in the estimation bound of a particular subset of the state $\mathbf{x} = \text{vec}\{\mathbf{x}_A, \mathbf{x}_S\}$, for example, only the state of the source \mathbf{x}_S . The total FIM can be divided into submatrices as

$$\mathbf{I}_{\mathbf{x}} = \begin{pmatrix} \mathbf{I}_{\mathbf{x}_A} & \mathbf{I}_{A_S} \\ \mathbf{I}_{S_A} & \mathbf{I}_{\mathbf{x}_S} \end{pmatrix} \quad (23)$$

where $\mathbf{I}_{\mathbf{x}_S}$ is the FIM of \mathbf{x}_S when the complementary set of parameter \mathbf{x}_A is perfectly known, that is

$$\text{CRB}[\mathbf{x}_S; \mathbf{x}_A] = \mathbf{I}_{\mathbf{x}_S}^{-1}. \quad (24)$$

When \mathbf{x}_A is unknown, the CRB of \mathbf{x}_S can be equivalently formulated by the so-called equivalent FI matrix (EFIM) [87] $\tilde{\mathbf{I}}_{\mathbf{x}_S}$ according to the Schur complement

$$\text{cov}_{\mathbf{z}}[\hat{\mathbf{x}}_S] \succcurlyeq \text{CRB}[\mathbf{x}_S] = \tilde{\mathbf{I}}_{\mathbf{x}_S}^{-1} \triangleq \left(\mathbf{I}_{\mathbf{x}_S} - \underbrace{\mathbf{I}_{S_A} \mathbf{I}_{\mathbf{x}_A}^{-1} \mathbf{I}_{A_S}}_{\triangleq \mathbf{D}_{\mathbf{x}_A \rightarrow \mathbf{x}_S}} \right)^{-1} \quad (25)$$

where the term \mathbf{I}_A is the FIM of the state of swarm \mathbf{x}_A , which has been thoroughly addressed in [34] within the content of network localization. The term $\mathbf{D}_{\mathbf{x}_A \rightarrow \mathbf{x}_S}$ represents the information degradation of \mathbf{x}_S from the uncertainty in \mathbf{x}_A . We are especially interested in challenging external source exploration applications, such as gas exploration [73] and returning to mission base [83]. In these applications, external sources are distant from the swarm with poor S2A measurement quality. Hence, their state estimates are often associated with high uncertainties. A large-scale swarm with high density is particularly beneficial for localizing these external sources. Agents in the swarm are close together and can thus acquire precise A2A measurements. Therefore, the state uncertainty of the swarm is much lower than the one of the external sources. In this case, the information degradation is negligible, and the unconditional CRB $[\mathbf{x}_S]$ can be approximated by the conditional CRB $[\mathbf{x}_S; \mathbf{x}_A]$. We can thus investigate source localization assuming that the state of the swarm is given. We can also exploit the different position uncertainty levels of the swarm and the external sources for the design of a swarm control strategy. For example, the swarm can actively forage position information of external sources (information seeking as a cost function), while constraining its own position uncertainty to a low level (information seeking as constraints). This swarm control strategy is demonstrated in the case study in Section V-B.

The Schur complement is also essential in the derivation of the PCRb, where the parameters \mathbf{x} are considered as random variables and estimated incorporating *a priori* information and the sequential measurements $\mathbf{z}^{(1:+)}$. The PCRb lower bounds the covariance matrix of a Bayesian estimation $\hat{\mathbf{x}}$, and is expressed by inverting the BIM $\mathbf{J}_{\mathbf{x}}^{(+)}$, that is

$$\text{cov}_{\mathbf{x}^{(+)}, \mathbf{z}^{(0:+)}}[\hat{\mathbf{x}}] \succcurlyeq \text{PCRb}[\mathbf{x}] \triangleq (\mathbf{J}_{\mathbf{x}}^{(+)})^{-1}. \quad (26)$$

In general, the BIM can be calculated recursively as [39]

$$\mathbf{J}_{\mathbf{x}}^{(+)} = \mathbf{D}_{22} - \mathbf{D}_{21} (\mathbf{J}_{\mathbf{x}}^{(-)} + \mathbf{D}_{11})^{-1} \mathbf{D}_{12} \quad (27)$$

where

$$\mathbf{D}_{11} = \mathbb{E}_{\mathbf{x}^{(-)}, \mathbf{x}^{(+)}} [-\Delta_{\mathbf{x}^{(-)}}^{\mathbf{x}^{(-)}} \ln p(\mathbf{x}^{(+)} | \mathbf{x}^{(-)})] \quad (28)$$

$$\mathbf{D}_{12} = \mathbb{E}_{\mathbf{x}^{(-)}, \mathbf{x}^{(+)}} [-\Delta_{\mathbf{x}^{(-)}}^{\mathbf{x}^{(+)}} \ln p(\mathbf{x}^{(+)} | \mathbf{x}^{(-)})] = \mathbf{D}_{21}^T \quad (29)$$

$$\begin{aligned} \mathbf{D}_{22} = & \mathbb{E}_{\mathbf{x}^{(-)}, \mathbf{x}^{(+)}} [-\Delta_{\mathbf{x}^{(+)}}^{\mathbf{x}^{(+)}} \ln p(\mathbf{x}^{(+)} | \mathbf{x}^{(-)})] \\ & + \underbrace{\mathbb{E}_{\mathbf{x}^{(+)}} [\mathbb{E}_{\mathbf{z}^{(+)}} [\mathbf{J}_{\mathbf{x}^{(+)}}] \ln p(\mathbf{z}^{(+)} | \mathbf{x}^{(+)})]}_{\mathbf{I}_{\mathbf{x}}^{(+)}}. \end{aligned} \quad (30)$$

The term $\mathbf{I}_{\mathbf{x}}^{(+)}$ represents the information about $\mathbf{x}^{(+)}$ in the current measurements $\mathbf{z}^{(+)}$, which has an identical expression as the FIM $\mathbf{I}_{\mathbf{x}}$ in the non-Bayesian case.

Exploiting the theory of FI, we infer descriptive geometrical interpretations of the swarm source localization problem in Section III-B. Going one step further, since the CRB and PCRb are closely related to the variance of parameter estimation, they can be utilized for information seeking swarm control, which we discuss in Section IV.

B. Source Localization by a Swarm

As a next step, we apply the FI theory to analyze the decisive impact factors in swarm source localization. We assume a generic source $\mathbf{o}_v \in \mathcal{S}$ distant from the swarm emits a radial signal $s_v(t)$, which is received by all agents. In this section, we consider the agents' state \mathbf{x}_A to be known and focus on the source localization problem. Swarm source localization can be equivalently seen as two problems, namely determining the distance d_v and the AoA θ_v of the source w.r.t. the swarm center. In order to assess the properties of the two problems separately, we rewrite the agent and source positions in the swarm polar coordinate system \mathbb{P} , with the pole located at the swarm center and a nonspecific reference direction, since the reference direction will not affect the geometrical interpretation of the source localization CRB. The polar coordinates of agents and sources are $\mathbf{p}_u^{\mathbb{P}} = \text{vec}\{d_u, \theta_u\}$, $\forall \mathbf{o}_u \in \mathcal{A}$ and $\mathbf{p}_v^{\mathbb{P}} = \text{vec}\{d_v, \theta_v\}$, respectively. In this section, the swarm polar coordinate system \mathbb{P} is used as the default coordinate system. Therefore, the superscript

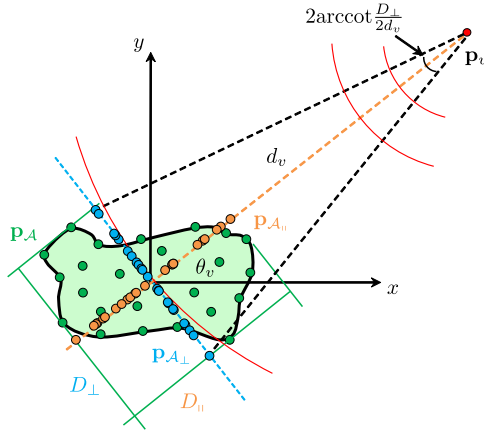


Fig. 3. Graph representation of swarm source localization: Red marker indicates a source, green markers indicate agents. Orange and cyan markers indicate radial and tangential projections of the agents, respectively. The radial and tangential aperture length $D_{||}$ and D_{\perp} as well as the opening angle of the aperture $2\text{arccot} D_{\perp}/2d_v$ are illustrated.

of \mathbb{P} is omitted for simplicity. We generally assume some nuisance parameters \mathbf{a}_v , which need to be jointly estimated with the source position. The joint state vector to be estimated is thus $\mathbf{x}_v = \text{vec}\{\mathbf{p}_v, \mathbf{a}_v\}$. The source localization performance is decisively determined by the geometry of the swarm aperture and the observation models. A graphical representation of swarm source localization and the key characteristics of the aperture are illustrated in Fig. 3. The swarm aperture can be decomposed into the radial (along the source AoA) and tangential (orthogonal to the source AoA) direction of the signal, which we refer to as the radial aperture with length $D_{||}$ and the tangential aperture with length D_{\perp} , respectively. The two directional apertures play distinguished roles in source localization, which can be analyzed by projecting the agent position \mathbf{p}_u onto the radial direction as $\mathbf{p}_{u,||} = \text{vec}\{d_{u,||}, \theta_{u,||}\}$ with $\mathbf{p}_{\mathcal{A}_{||}} = \text{vec}\{\mathbf{p}_{u,||} : \mathbf{u} \in \mathcal{A}\}$, as well as onto the tangential direction as $\mathbf{p}_{u,\perp} = \text{vec}\{d_{u,\perp}, \theta_{u,\perp}\}$ with $\mathbf{p}_{\mathcal{A}_{\perp}} = \text{vec}\{\mathbf{p}_{u,\perp} : \mathbf{u} \in \mathcal{A}\}$. The technique of using a linear array to approximate the performance of an arbitrary array is widely applied for example in source AoA estimation [88]. Another important aperture characteristic w.r.t. source localization is the angular aperture $D_{\perp}/2d_v$, analogous to the angular aperture of an optical lens. The angular aperture measures the opening angle of the swarm aperture toward the source, which shows the relative geometry of the joint swarm-source system.

1) *Collective View on Swarm Aperture:* The source state is written as $\mathbf{x}_v = \text{vec}\{\mathbf{p}_v, \mathbf{a}_v\}$. Analogous to (23) and Section III-A, the EFIM of \mathbf{p}_v , denoted as $\tilde{\mathbf{I}}_{\mathbf{p}_v}$, can be derived using the Schur complement as

$$\tilde{\mathbf{I}}_{\mathbf{p}_v} = \mathbf{I}_{\mathbf{p}_v} - \underbrace{\mathbf{I}_{\mathbf{p}_v, \mathbf{a}_v} \mathbf{I}_{\mathbf{a}_v}^{-1} \mathbf{I}_{\mathbf{p}_v, \mathbf{a}_v}^T}_{\mathbf{D}_{\mathbf{a}_v \rightarrow \mathbf{p}_v}} \quad (31)$$

where $\mathbf{I}_{\mathbf{p}_v}$ is the information about \mathbf{p}_v given the nuisance parameters \mathbf{a}_v . The term $\mathbf{D}_{\mathbf{a}_v \rightarrow \mathbf{p}_v}$ shows the degradation of the information about \mathbf{p}_v when \mathbf{a}_v is unknown. The components of (31) are defined as

$$\begin{aligned} \mathbf{I}_{\mathbf{p}_v} &= \sum_{\mathbf{u} \in \mathcal{A}} \iota_{g_{uv}} \left(\frac{\partial g_{uv}}{\partial d_{uv}} \right)^2 \nabla_{\mathbf{p}_v} d_{uv} \nabla_{\mathbf{p}_v}^T d_{uv} \\ \mathbf{I}_{\mathbf{p}_v, \mathbf{a}_v} &= \sum_{\mathbf{u} \in \mathcal{A}} \iota_{g_{uv}} \frac{\partial g_{uv}}{\partial d_{uv}} \nabla_{\mathbf{p}_v} d_{uv} \nabla_{\mathbf{a}_v}^T g_{uv} \\ \mathbf{I}_{\mathbf{a}_v} &= \sum_{\mathbf{u} \in \mathcal{A}} \iota_{g_{uv}} \nabla_{\mathbf{a}_v} g_{uv} \nabla_{\mathbf{a}_v}^T g_{uv}. \end{aligned} \quad (32)$$

For a large-scale swarm, the observability of certain parameters like a source position is decisively determined by the swarm collective aperture and the observation models. From a macroscopic perspective, a swarm with a massive number of agents in 2-D, that is, $|\mathcal{A}| \rightarrow \infty$, and a finite aperture size $D = 2R$, can be considered as a surface which captures signals in a spatially continuous manner. The agent positions \mathbf{p}_u can be treated as known independent and identically distributed (i.i.d.) random variables with a pdf $p(d_u, \theta_u)$. Hence, the summation of a certain function $f(d, \theta)$, sampled at every agent $f(d_u, \theta_u)$, $\forall \mathbf{u} \in \mathcal{A}$, can be approximated asymptotically by the expectation over the spatial distribution of the agents, that is

$$\lim_{|\mathcal{A}| \rightarrow \infty} \sum_{\mathbf{u} \in \mathcal{A}} f(d_u, \theta_u) = |\mathcal{A}| \mathbb{E}_{\mathbf{p}_u} [f(d_u, \theta_u)]. \quad (33)$$

With this approximation, we can rewrite (32) with expectations and focus on the collective aperture covered by the swarm, instead of a particular swarm formation. The collective view on the swarm aperture provides more insights into the geometrical interpretation of source localization, which will be discussed in Sections III-B2 and III-B3.

2) *Information Degraded by Nuisance Parameters:* From the models in Section II-C, we observe that the position information of an isotropic point source, that is, distance d_v and AoA θ_v from the swarm perspective, is inferred essentially from the distances d_{uv} between the source \mathbf{u}_v and the agents $\mathbf{u} \in \mathcal{A}$.

The AoA θ_v can be estimated utilizing the fact that signals emitted from an isotropic point propagate radially. The tangential line of the signal front, illustrated with a cyan dashed line in Fig. 3, is always perpendicular to the direction of the source (orange dashed line in Fig. 3). Especially when the source is distant from the swarm, the signal front is approximately planar. Agents along the tangential line will observe nearly identical signal values. Intuitively, the AoA of the source can be fully determined from the directions of these lines, independently of the knowledge of the nuisance parameters. Hence the AoA information of a distant source can be captured only by the tangential

aperture of the swarm. In fact, particularly for a planar phased array with arbitrary geometry like \mathbf{p}_A in Fig. 3, the source AoA estimation CRB can be approximated by one of the projected tangential linear arrays \mathbf{p}_{A_\perp} in Fig. 3. This result can be proved by combining [89, p. 37] and [90, p. 659].

When using the plane wave assumption (planar signal front), the distance information of a distant source is solely contained in the observation from the radial aperture, since the signal feature $g_{uv} = g(d_{uv}, \mathbf{a}_v)$ contains only distinguishable values in the radial direction. Therefore, we look into the source distance observability with the linear radial swarm position projection \mathbf{p}_{A_\parallel} . If the nuisance parameters are known, the distance between source and agent d_{uv} can be directly derived from a signal feature $g_{uv} = g(d_{uv})$. The source to swarm distance d_v can be estimated by averaging over the range measurements from all agents.

The rest of this section is dedicated to the general case where an unknown nuisance parameter is present. We consider a generic signal feature $g_{uv} = g(d_{uv}, a_v)$ as an arbitrary function of the source to agent distance d_{uv} and a single nuisance parameter a_v . We prove that a nuisance parameter can be separated from the source distance by the radial aperture, unless the nuisance parameter is additive to the S2A distance, like the propagation time based signal features listed in Table 2.

Let us consider a linear swarm, that is, a swarm composed of agents on a line along the x -axis with known positions in polar coordinate system \mathbf{p}_A . A source is located on the positive x -axis at distance d_v from the swarm, that is, $\theta_v = 0$ and known. Let us further assume the signal feature at agent \mathbf{p}_u is $g_{uv} = g(d_v - x_u, a_v)$. The FIM of $\mathbf{x}_v = \text{vec}\{d_v, a_v\}$ is then approximated with expectation as

$$\mathbf{I}_{\mathbf{x}_v} \approx |\mathcal{A}| \mathbb{E}_{\mathbf{p}_u} \left[\iota_{g_{uv}} \begin{pmatrix} \left(\frac{\partial g_{uv}}{\partial d_v} \right)^2 & \frac{\partial g_{uv}}{\partial d_v} \frac{\partial g_{uv}}{\partial a_v} \\ \frac{\partial g_{uv}}{\partial d_v} \frac{\partial g_{uv}}{\partial a_v} & \left(\frac{\partial g_{uv}}{\partial a_v} \right)^2 \end{pmatrix} \right]. \quad (34)$$

The source distance is not observable if and only if (i.f.f.)

$$\det[\mathbf{I}_{\mathbf{x}_v}] = 0 \quad (35)$$

which leads to the following lemma.

Lemma 1 (PDE Condition of Source Localizability): A linear swarm cannot observe its distance to a collinear source d_{uv} and a nuisance parameter a_v i.f.f. the following PDE holds:

$$G \frac{\partial g(d_{uv}, a_v)}{\partial d_{uv}} = \frac{\partial g(d_{uv}, a_v)}{\partial a_v} \quad (36)$$

where G is an arbitrary constant coefficient.

Proof: See Appendix A. \square

The PDE in (36) belongs to the class of first-order PDE with a constant coefficient. Discarding the trivial solution of $g(d_{uv}, a_v) = C$, the general solution of this type of PDE is expressed in [91, p. 359] as

$$g(d_{uv}, a_v) = F(d_{uv} + Ga_v) \quad (37)$$

where $F(\xi)$ is any differentiable function of a single variable ξ . With this observation, the following proposition can be readily stated.

Proposition 1 (Necessary and Sufficient Condition of Source Localizability by a Collinear Swarm): A linear swarm is able to observe the distance to a collinear source d_{uv} and a nuisance parameter a_v i.f.f. the signal feature function $g(d_{uv}, a_v)$ possesses a form other than (37).

This proposition can be interpreted such that for an unknown nuisance parameter additive to the S2A distance, for example, a clock offset for ToA, or a carrier phase offset for phase of arrival (PoA), the source distance cannot be observed with the planar signal model. For arbitrary types of signal feature $g(d_{uv}, a_v)$ other than the class defined by (37), the distance to a collinear source can still be estimated by the linear swarm with a reduced accuracy compared to the case of known nuisance parameter. One example is the gas concentration with scaling and exponent factors as nuisance parameters, introduced in (15).

Even for the additive nuisance parameter case, where the source distance is not distinguishable from a nuisance parameter with the planar signal model, it can be estimated by the observations from the tangential aperture with radial signal model. This technique utilizes the signal CoA and performs well for short-to-moderate source distance as discussed in [36].

In Section III-B3, we provide a geometrical interpretation of the extractable source position information from the signal CoA.

3) Source Localization With Radial Signal Model: The concept of CoA-based source distance estimation is intuitively illustrated by a toy example in Fig. 4. A source located at \mathbf{p}_v transmits a real-valued signal like a sine wave in Fig. 4, that is, $s_{uv}(\|\mathbf{p}_u - \mathbf{p}_v\|; t) = \sin(t - \|\mathbf{p}_u - \mathbf{p}_v\|/c)$. The signal propagates to the swarm as illustrated by the red curve. From the view of the radial swarm aperture (orange section), the received signal would be identical to the one (blue curve) transmitted at an offsetted position $\tilde{\mathbf{p}}_v$ with a corresponding delay offset δ . Contrarily, from the view of the tangential aperture (cyan section), the offsetted position $\tilde{\mathbf{p}}_v$, which is closer to the swarm compared to the true position \mathbf{p}_v , intuitively leads to a higher curvature of the signal front. Hence, the source distance can be determined uniquely.

Now, we quantify the extractable distance information from the CoA. We assume a single nuisance parameter a_v and a signal feature $g(d_{uv}, a_v) = g(d_{uv} + Ga_v)$ fulfilling (37). The source state is written as $\mathbf{x}_v = \text{vec}\{\mathbf{p}_v, a_v\}$. Additionally, we assume the source distance is much

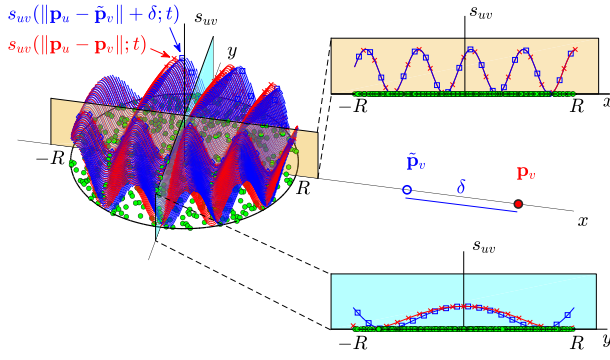


Fig. 4. Observability of source distance d_v in the presence of a distance offset δ as nuisance parameter: d_v and δ are not separable by the radial aperture (orange section), but are separable through observing the CoA by the tangential aperture (cyan section).

larger than the size of the swarm, i.e., $d_v \gg \max\{d_u : \forall \mathbf{p}_u \in \mathcal{A}\}$, so that $\iota_{g_{uv}}$ and $\partial g(d_{uv}, a_v)/\partial d_v$ are approximated by their values at $d_{uv} = d_v$. Applying the Schur complement, the position EFIM of the source $\tilde{\mathbf{I}}_{\mathbf{p}_v}$ can be approximated as

$$\tilde{\mathbf{I}}_{\mathbf{p}_v} \approx \iota_{d_v} |\mathcal{A}| \mathbb{E}_{\mathbf{p}_u} [\nabla_{\mathbf{p}_v} d_{uv} \nabla_{(\mathbf{p}_v)^T} d_{uv}] - \iota_{d_v} |\mathcal{A}| \mathbb{E}_{\mathbf{p}_u} [\nabla_{\mathbf{p}_v} d_{uv}] \mathbb{E}_{\mathbf{p}_u} [\nabla_{(\mathbf{p}_v)^T} d_{uv}] \quad (38)$$

where ι_{d_v} is the RII at the swarm center defined as

$$\iota_{d_v} \triangleq \iota_{g_{uv}} \left(\frac{\partial g_{uv}}{\partial d_{uv}} \right)^2 \bigg|_{d_{uv}=d_v} \quad (39)$$

Besides, the S2A distance d_{uv} is approximated by its second-order Taylor expansion around $d_u = 0$ as

$$d_{uv} \approx d_v - d_u \cos(\theta_u - \theta_v) + \frac{d_u^2}{2d_v} \sin^2(\theta_u - \theta_v). \quad (40)$$

Additionally, we consider a large-scale swarm, whose agents are randomly located on a disk centered at the origin with radius R . The positions of the agents are statistically i.i.d.. They are distributed uniformly in the corresponding swarm Cartesian coordinate system, within a disk of radius R . In Fig. 5 the green markers illustrate a realization of the positions of 50 agents. With the approximation in (38)–(40) and the uniformly i.i.d. agents positions, a further approximation of the EFIM of the source position $\mathbf{p}_v = \text{vec}\{d_v, \theta_v\}$ can be obtained, after some algebra, as

$$\tilde{\mathbf{I}}_{\mathbf{p}_v} \approx \iota_{d_v} |\mathcal{A}| \underbrace{\begin{pmatrix} \frac{32d_v^4 - 8d_v^2 R^2 + R^4}{32d_v^4} & 0 \\ 0 & \frac{6d_v^2 R^2 + R^4}{24d_v^2} \end{pmatrix}}_{\approx \mathbf{I}_{\mathbf{p}_v}}$$

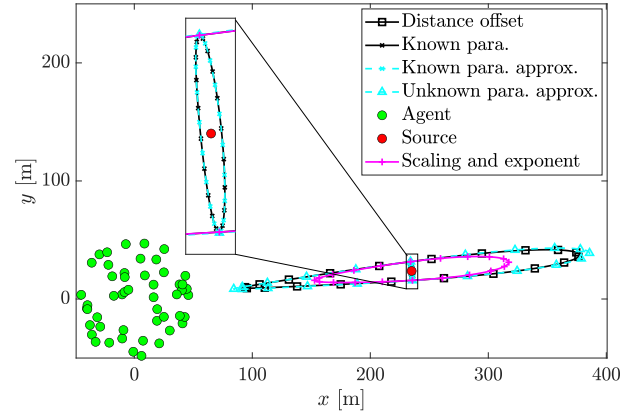


Fig. 5. Comparison of the 6σ source position CRB in polar coordinates for the cases of known and unknown nuisance parameters, i.e., scaling and exponent factors or distance offset.

$$- \iota_{d_v} |\mathcal{A}| \underbrace{\begin{pmatrix} \frac{64d_v^4 - 16d_v^2 R^2 + R^4}{64d_v^4} & 0 \\ 0 & 0 \end{pmatrix}}_{\approx \mathbf{D}_{a_v \rightarrow \mathbf{p}_v}} \quad (41)$$

where $\mathbf{I}_{\mathbf{p}_v}$ is the FIM assuming a known nuisance parameter. Applying the assumption of $d_v \gg R$ leads to the nonmatrix-inversion CRB approximations as follows.

Theorem 1 (Nuisance Parameter Impact on Source Localization CRBs): For a swarm estimating a source position $\mathbf{p}_v = \text{vec}\{d_v, \theta_v\}$ with the presence of a known nuisance parameter a_v additive to the S2A distance d_{uv} , the CRB of \mathbf{p}_v is approximated by

$$\text{CRB}[\mathbf{p}_v; a_v] \approx \frac{1}{\iota_{d_v} |\mathcal{A}|} \begin{pmatrix} 1 & 0 \\ 0 & \frac{4}{R^2} \end{pmatrix}. \quad (42)$$

If the additive nuisance parameter is unknown, the CRB of \mathbf{p}_v is approximated by

$$\text{CRB}[\mathbf{p}_v] \approx \frac{1}{\iota_{d_v} |\mathcal{A}|} \begin{pmatrix} 64 \left(\frac{d_v}{R} \right)^4 & 0 \\ 0 & \frac{4}{R^2} \end{pmatrix}. \quad (43)$$

The first diagonal entries $\text{CRB}[d_v; a_v] = \text{CRB}[\mathbf{p}_v; a_v]_{(1,1)}$ and $\text{CRB}[d_v] = \text{CRB}[\mathbf{p}_v]_{(1,1)}$ are the source distance estimation lower bounds with known and unknown nuisance parameters, respectively. The second diagonal entries $\text{CRB}[\theta_v; a_v] = \text{CRB}[\mathbf{p}_v; a_v]_{(2,2)}$ and $\text{CRB}[\theta_v] = \text{CRB}[\mathbf{p}_v]_{(2,2)}$ are the corresponding source AoA estimation lower bounds. The AoA estimation variance is inverse quadratically proportional to the aperture radius R and independent of the knowledge of nuisance parameter. Contrarily, the unknown nuisance parameter severely degrades the distance estimation, as the distance estimation variance in that case is inverse quartically (with fourth power) proportional to the angular aperture $D_{\perp/2} d_v = R/d_v$. The source position CRB

often additionally depends on d_v , through the impact to ι_{d_v} as addressed in [36]. Theorem 1 exams the impacts of collective aperture on source localization by assuming uniformly deployed agents. In [36], the favorable spatial distribution of the tangentially projected agent's position $\mathbf{p}_{A\perp}$ is discussed, which is another decisive factor to source localization. It has been proven that the source AoA bound $\text{CRB}[\theta_v]$ is inversely proportional to M_2 , where $M_n = \sum_{\mathbf{q}_u \in \mathcal{A}} (d_{u,\perp}/D_\perp)^n / |\mathcal{A}|$ is the n th empirical moment of agents' spatial distribution on the tangential aperture. The source distance bound $\text{CRB}[d_v]$ is inversely proportional to $M_4 - M_2^2$.

As discussed in Section III-B2, having an unknown nuisance parameter additive to the S2A distance is the worst case scenario in the sense of source distance estimation. Fig. 5 illustrates the effects of different types of nuisance parameters on source localization. The case of a single unknown additive nuisance parameter as defined in (37) is shown in black with square markers. The case of two unknown nuisance parameters with scaling $a_1 = 1$ and exponent factors $a_2 = -1$, i.e., $g(d_{uv}, a_1, a_2) = F(a_1 d_{uv}^{a_2})$ is shown with magenta curves. This model is closely related to energy intensity based observations, such as signal amplitude and gas concentration. The case of known nuisance parameter is shown in black with star markers. In addition, the approximated CRBs in (42) and (43) are plotted in cyan with star and triangle markers. As expected, the AoA accuracy is not affected by the nuisance parameters. With known nuisance parameters, approximated and true CRBs coincide. The AoA uncertainty is the main source of position estimation error. With unknown nuisance parameters, the distance CRB approximation matches the one of additive nuisance parameter well. Hence, the distance uncertainty becomes the main error source of position estimation. In the case of unknown scaling and exponent factors as nuisance parameters, the distance CRB is larger than the known parameter case and smaller than the additive nuisance parameter case, since the source distance can be also estimated by the radial aperture.

C. Summary of Swarm Localization

Before moving to swarm control, we summarize the main theoretical findings from this section w.r.t. swarm localization.

- The performance of swarm localization, especially external source localization, is decisively determined by the aperture of the swarm.
- The source AoA is observable mainly with the tangential aperture of the swarm, independently of the knowledge and type of nuisance parameters.
- For known nuisance parameters, the source distance can be estimated independently of the aperture.
- For an unknown nuisance parameter which is additive to the S2A distance, that is, $g(d_{uv}, a_v) = F(d_{uv} + G a_v)$, the source distance can only be observed from the tangential aperture of the swarm through the curvature of the signal front. The source distance

estimation accuracy is degraded the most with this type of unknown nuisance parameter.

- For other unknown nuisance parameters, the source distance can be observed from both tangential and radial aperture of the swarm. The estimation performance is between the cases of unknown additive nuisance parameter and known nuisance parameters.

These conclusive findings coincide with the collective behavior emerging from the information seeking swarm control introduced in Section IV, which will be discussed in the case study in Section V.

IV. INFORMATION SEEKING SWARM CONTROL

For traditional navigation systems, the control objectives are externally defined, optionally tolerating the state estimation uncertainty. Contrarily, in our autonomous swarm navigation system the estimation uncertainty is a controllable feature. The swarm is aware not only of the state estimation uncertainty but also of the causality between its states and the estimation uncertainty. With the later self-awareness, the swarm can actively adapt its formation minimizing the estimation uncertainty, meantime achieving other control objectives, such as goal approaching and collision avoidance.

We propose an information seeking swarm control concept based on projected steepest gradient descent (PSGD) algorithm. The FI or BI is utilized to construct information seeking objectives. Position CRBs or PCRBS of an arbitrary subset of nodes are employed as the cost function or the constraints of the control problem. Thus, the controller can be designed flexibly according to applications. A closed form expression of the gradient based controller is derived to enable low complexity swarm control.

As an example in this section, we consider the following movement model for the agents [55]:

$$\mathbf{p}_u^{(+)} = \mathbf{p}_u^{(-)} + \mathbf{b}_u + \boldsymbol{\omega}_u \quad \forall \mathbf{q}_u \in \mathcal{A} \quad (44)$$

that is the control command \mathbf{b}_u is directly applied to the 2-D position of the agent. This control command is constrained by a maximum step size b_{\max} , i.e., $\mathbf{b}_u \in \mathcal{U} = \{\mathbf{b}_u : \forall \|\mathbf{b}_u\| \leq b_{\max}\}$. In other words, the spatial movement between two time steps is limited. In addition, the control command is disturbed by additive Gaussian noise, that is

$$\boldsymbol{\omega}_u \sim \mathcal{N}(\mathbf{0}, \mathbf{Q}_u(\mathbf{b}_u)) \quad \forall \mathbf{q}_u \in \mathcal{A}. \quad (45)$$

The Gaussian noise has zero mean and its covariance is a function of the control command \mathbf{b}_u , for example,

$$\mathbf{Q}_u(\mathbf{b}_u) = \sigma_0^2 \|\mathbf{b}_u\| \otimes \mathbf{I}_{2 \times 2} \quad \forall \mathbf{q}_u \in \mathcal{A} \quad (46)$$

where σ_0^2 is the variance of noise normalized to step size. The transition covariance matrix of the complete state

is given by the diagonal matrix $\mathbf{Q}(\mathbf{b}_A)$, aggregating the diagonal elements of $\mathbf{Q}_u(\mathbf{b}_u)$, $\forall \mathbf{u}_u \in \mathcal{A}$ for the position of swarm, and zeros for the static parameters.

This transition model reflects the fact that if the traveled distance, that is, the magnitude of the control command, is large, so is the disturbance employed on this control. This is a realistic assumption for a high level movement model of a robot whose low level controller is based on odometry suffering from drift. The considered transition model allows us to focus on demonstrating the concept of information seeking swarm control. Nonlinear state transition model can be taken into account for example by iterative linear quadratic regulator (ILQR) [92] and would not change the overall information seeking concept presented in this article.

A. Objective Functions for Swarm Control

Swarm control is often a multiobjective problem. These objectives act as cost functions denoted with letter f or constraints denoted with letter h , depending on their priorities defined by the applications. In this article, we consider three objectives, namely goal approaching, collision avoidance and position information seeking. The first two objectives are external mission objective exploiting the knowledge of position estimates, and optionally the estimation uncertainty. The position information seeking is an internal objective, reflecting the self-awareness of the swarm navigation system.

Goal approaching is a frequently applied objective for a wide variety of swarm control applications. A swarm aims to move from its current position $\mathbf{p}_A^{(-)}$ to a goal position \mathbf{p}_g , for example, the gas source position $\mathbf{p}_v, \mathbf{v}_v \in S_{\text{gas}}$ in the Mars exploration mission illustrated in Fig. 1. The objective of goal approaching is formulated preferably as a cost function like [93]

$$f_g(\mathbf{b}_A) = -\mathbf{b}_A^T \cdot \mathbf{e}_g \quad (47)$$

where

$$\mathbf{e}_g = \frac{\mathbf{1}_{|\mathcal{A}| \times 1} \otimes \mathbf{p}_g - \mathbf{p}_A}{\|\mathbf{1}_{|\mathcal{A}| \times 1} \otimes \mathbf{p}_g - \mathbf{p}_A\|}. \quad (48)$$

The Kronecker product stacks the goal position \mathbf{p}_g into a vector with the same size as \mathbf{p}_A . The goal approaching cost function reaches its minimum value when \mathbf{b}_A is aligned with \mathbf{e}_g . Hence, the preferable directions for goal approaching point to the goal from individual agents, which is intuitive.

Collision avoidance is another crucial objective for swarm control. Due to the imperfection of the controller and the position uncertainty, an agent $\mathbf{u}_u \in \mathcal{A}$ need to keep its distance d_{uv} to another node $\mathbf{u}_v \in \mathcal{V}$ larger than a minimal tolerated distance d_{\min} . The collision avoidance objective is preferably written as a constraint

$$h_{c,uv}(\mathbf{b}_A) \geq 0 \quad \forall \mathbf{u}_u \in \mathcal{A}, \mathbf{u}_v \in \mathcal{V}/\mathbf{u}_u. \quad (49)$$

The objective function $h_{c,uv}(\mathbf{b}_A)$ can either be written in a deterministic fashion as in [83], [93]

$$d_{uv} - d_{\min} \geq 0 \quad (50)$$

where in practice the distance d_{uv} is replaced with its estimate $\|\hat{\mathbf{p}}_u - \hat{\mathbf{p}}_v\|$, or with a stochastic expression

$$h_{c,uv}(\mathbf{b}_A) \triangleq \beta_{\max} - \Pr[d_{uv} \leq d_{\min}] \geq 0 \quad (51)$$

where $\Pr[d_{uv} \leq d_{\min}]$ denotes the probability of $d_{uv} \leq d_{\min}$, $\beta_{\max} \in [0, 1]$ is the maximum acceptable probability of the violation of the minimum tolerated distance d_{\min} . The probability in (51) can be evaluated by the position CRB or PCRB together with the multivariate Chebyshev inequality introduced in [94].

Position information seeking objective, as a main contribution of this article, aims at manipulating the swarm to a favorable position, where the predicted measurements $\tilde{\mathbf{z}}^{(+)}$ provide the richest additional information on the state. The state estimation covariance matrix, calculated from $p(\tilde{\mathbf{z}}^{(+)}; \mathbf{x}^{(+)})$ for FI seeking or from $p(\mathbf{x}^{(+)} | \mathbf{z}^{(1:-)}, \tilde{\mathbf{z}}^{(+)})$ for BI seeking, is utilized to construct the information seeking objectives. Different figure of merits of the covariance matrix can be exploited as the optimization criterion [64]. D-, E-, and A-optimalities minimize the determinant, the maximum eigenvalue and the trace of the covariance matrix, which can be interpreted as minimizing the volume, the largest dimension and the average size of the covariance ellipsoid, respectively. In this article, we use the trace of the weighted covariance matrix of the total state estimation, as the design criterion. The subscript of the pdf $p(x)$ indication in $\text{cov}_x[\dots]$ is omitted for generic information seeking objective formulation. Position information seeking can be written as a cost function

$$f_p(\mathbf{b}_A) \triangleq \text{tr}[\mathbf{\Lambda} \text{cov}[\hat{\mathbf{x}}^{(+)}]] \quad (52)$$

where the diagonal weighing matrix $\mathbf{\Lambda} = \text{diag}\{\lambda_i : i = 1, \dots, N_x\}$ indicates the objective emphasis on the N_x dimensional state space. The entities λ_i of the weighing matrix can be either binary valued from $\{0, 1\}$ to select certain dimensions of the state for optimization, or arbitrary nonnegative real value, which puts different weights at particular dimensions. The weights on nonposition states are set to zero. We introduce a notation $\mathbf{\Lambda}_{\mathcal{P}}$ as the weighing matrix with ones for the positions of nodes in set \mathcal{P} , and zeros for other state. With the cost function $f_p(\mathbf{b}_A)$, the swarm will constantly optimize its position so that the value of this cost function gradually decreases.

The position information seeking objective can also be formulated as $l = 1, \dots, L_p$ constraints, which are only activated, if the value of the objective function is not

smaller a certain maximum tolerated position error $\varepsilon_{\max,l}$, that is

$$h_{p,l}(\mathbf{b}_A) \triangleq \varepsilon_{\max,l} - \text{tr}[\Lambda_l \text{COV}[\hat{\mathbf{x}}^{(+)}]] \geq 0, \quad l = 1, \dots, L_p \quad (53)$$

where Λ_l is the weighing matrix of the l th information seeking constraint, expressed similarly as Λ .

The information seeking cost function and constraints can be flexibly combined, adapting the application criteria. For example, in the gas source exploration mission illustrated in Fig. 1, the swarm can set the gas source position uncertainty as the information seeking cost function, and the position uncertainty of agents as constraints.

The covariance matrix is an empirical metric, which is difficult to be directly exploited as an objective function for two reasons. First, a large number of samples are demanded to evaluate the covariance matrix. Second, even if a covariance matrix has been calculated from samples, it cannot be analytically formulated as a differentiable function to generate a control command \mathbf{b}_A . In Sections IV-C and IV-D, we use FI and BI to predict the covariance matrices in the design of information seeking swarm controls.

By combining the introduced objective functions, the self-aware swarm control problem can be formulated, for example, by the commonly employed weighted sum method [95]. A linear combination of cost functions $f_p(\mathbf{b}_A)$ and $f_g(\mathbf{b}_A)$ with weight w_p and w_g as the total cost function is minimized, subject to (s.t.) multiple constraints, that is

$$\min_{\mathbf{b}_A \in \mathcal{U}_A} \underbrace{w_p f_p(\mathbf{b}_A)}_{\text{(information seeking)}} + \underbrace{w_g f_g(\mathbf{b}_A)}_{\text{(goal approaching)}} \quad (54a)$$

s.t. information seeking:

$$h_{p,l}(\mathbf{b}_A) \geq 0, \quad l = 1, \dots, L_p \quad (54b)$$

collision avoidance:

$$h_{c,uv}(\mathbf{b}_A) \geq 0 \quad \forall \mathbf{u}_u \in \mathcal{A}, \mathbf{u}_v \in \mathcal{V}/\mathbf{u}_u. \quad (54c)$$

The feasible control command set \mathcal{U}_A can be interpreted as a constraint as well. However, since it acts on the travel distance instead of direction, we consider it separately from the other constraints. The problem formulation in (54) is designed for homogeneous swarm control strategy. It can be straightforwardly extended to a heterogeneous swarm control strategy like leader-follower control, where the cost functions and the constraints are designed differently for each individual agent.

B. Gradient Descent Swarm Control

For the considered large-scale swarm, the swarm control problem formulated in (54) is a high-dimensional nonconvex optimization problem. Instead of finding the optimal solution in one step, we adapt the PSGD method [96, Ch. 5] to design a low complexity swarm controller.

PSGD is an iterative method to find a locally optimal solution of a constrained optimization problem. The general idea of PSGD is to iteratively apply the following three steps: i) defining initial solution with the steepest gradient descent of the cost function; ii) constraining the initial solution onto the tangent space of the potentially violated constraints; and iii) applying necessary corrections to compensate the nonlinearity effect of the constraints. We utilize the general concept of PSGD to generate the control command \mathbf{b}_A for the swarm from the gradients of the cost function and the constraints. As previously stated, the PSGD applies an iterating-till-convergence strategy to obtain solutions of optimization problems. Instead, in the proposed swarm control, the cost function and the constraints are evaluated only once at the current swarm position to find an optimized control command \mathbf{u}_A . The agents move according to \mathbf{u}_A . Then the new command is generated at the next time step. With this modification, a low complexity can be maintained for real-time swarm control, at a risk of possible slight constraint violations. For the simplicity of the controller description, we reformulate (54) to a generic optimization problem with a cost function $f(\mathbf{b}_A)$ and L inequality constraints $\mathbf{h}(\mathbf{b}_A) \geq \mathbf{0}$, where $\mathbf{h}(\mathbf{b}_A) = \text{vec}\{h_l(\mathbf{b}_A) : l = 1, \dots, L\}$, that is

$$\min_{\mathbf{b}_A \in \mathcal{U}_A} f(\mathbf{b}_A) \quad (55)$$

$$\text{s.t. } \mathbf{h}(\mathbf{b}_A) \geq \mathbf{0}. \quad (56)$$

The gradient of the objective function is written as

$$\mathbf{c}_A = \text{vec}\{\mathbf{c}_u : \mathbf{u}_u \in \mathcal{A}\} = \nabla_{\mathbf{b}_A} f(\mathbf{b}_A) \quad (57)$$

which points to the direction where the value of $f(\mathbf{b}_A)$ ascends steepest. An unconstrained control command $\tilde{\mathbf{b}}_A$ can first be found by the steepest gradient descent method similar to step i) of PSGD as

$$\tilde{\mathbf{b}}_A = \text{vec}\{\mathbf{c}_u : \mathbf{u}_u \in \mathcal{A}\} = -\mu \frac{\mathbf{c}_A}{\|\mathbf{c}_A\|} \quad (58)$$

where μ is the chosen step size of the gradient descent, such that $\max\{\|\mathbf{b}_u\| : \mathbf{u}_u \in \mathcal{A}\} \leq b_{\max}$. The maximum travel distance in one step is denoted as b_{\max} , which is limited by the mechanical capability of the agents. Then we identify the activated constraint vector $\mathbf{h}_a(\mathbf{b}_A) = \text{vec}\{h_l(\mathbf{b}_A) : h_l(\mathbf{0}) \leq 0\}$ with length L_a , that is, the constraints that either have been violated or are at the boundary of violation. The constraint gradient matrix $\mathbf{N} \in \mathbb{R}^{2|\mathcal{A}| \times L_a}$ is a $2|\mathcal{A}| \times L_a$ real-valued matrix defined as

$$\mathbf{N} = \nabla_{\mathbf{b}_A} \mathbf{h}_a(\mathbf{b}_A)^T|_{\mathbf{b}_A=\mathbf{0}}. \quad (59)$$

A projection matrix $\mathbf{P} \in \mathbb{R}^{2|\mathcal{A}| \times 2|\mathcal{A}|}$ is defined as

$$\mathbf{P} = \mathbf{I} - \mathbf{N}(\mathbf{N}^T \mathbf{N})^{-1} \mathbf{N}^T \quad (60)$$

which projects the unconstrained control command $\tilde{\mathbf{b}}_{\mathcal{A}}$ onto the tangent space of the activated constraints. The control command δ after the projection is expressed as

$$\delta = \mathbf{P}\tilde{\mathbf{b}}_{\mathcal{A}}. \quad (61)$$

In addition, the quantity of constraint violations need to be compensated, which leads to the solution of the control command, similar to step ii) of PSGD, as

$$\mathbf{b}_{\mathcal{A}} = \delta - \mathbf{N}(\mathbf{N}^T \mathbf{N})^{-1} \mathbf{h}_{\mathbf{a}}(\mathbf{0}). \quad (62)$$

A scaling factor may be applied again if $\mathbf{b}_{\mathcal{A}}$ is not contained in the feasible set of control command $\mathcal{U}_{\mathcal{A}}$ due to the compensation step.

From the problem definition in (54) and (55), and algorithm step description in (57)–(62), we can observe that the essence of applying such an algorithm is firstly to design the cost function $f(\mathbf{b}_{\mathcal{A}})$ and the constraints $\mathbf{h}(\mathbf{b}_{\mathcal{A}})$, and secondly to calculate $\mathbf{c}_{\mathcal{A}}$ in (57) and \mathbf{N} in (59) from the derivatives of the cost function $f(\mathbf{b}_{\mathcal{A}})$ and the activated constraints $\mathbf{h}_{\mathbf{a}}(\mathbf{b}_{\mathcal{A}})$ w.r.t. the control command $\mathbf{b}_{\mathcal{A}}$. Calculating the gradients of the goal approaching and the collision avoidance objectives are straightforward and have been addressed in [83] and [93]. Therefore, the key of following information seeking objectives, either as a cost function or as constraints, is to derive the gradients of the CRB and PCRB, weighted by a diagonal matrix Λ , that is, $\nabla_{\mathbf{b}_{\mathcal{A}}} \text{tr}[\Lambda \text{CRB}[\mathbf{x}^{(+)}]]$ and $\nabla_{\mathbf{b}_{\mathcal{A}}} \text{tr}[\Lambda \text{PCRB}[\mathbf{x}^{(+)}]]$. These two gradients represent the knowledge of causality between the swarm positions and the state estimation uncertainty. In Sections IV-C and IV-D, instead of describing the complete swarm controllers, we will only focus on deriving the information seeking gradients.

C. FI Seeking

As discussed in Section IV-A, the estimation covariance is an empirical metric and not suitable to be directly used as the objective function. Instead, position information seeking objective functions can be formulated with the predicted FIM, denoted as $\mathbf{I}_{\mathbf{x}(+)}$, given a snapshot of predicted measurements $\tilde{\mathbf{z}}^{(+)}$, that is, virtual measurements expected to be obtained at the new position. The predicted CRB, denoted as $\text{CRB}[\mathbf{x}^{(+)}]$, is a lower bound of the predicted estimation covariance $\text{cov}_{\tilde{\mathbf{z}}(+)}[\hat{\mathbf{x}}^{(+)}]$, that is

$$\text{cov}_{\tilde{\mathbf{z}}(+)}[\hat{\mathbf{x}}^{(+)}] \succcurlyeq \text{CRB}[\mathbf{x}^{(+)}]. \quad (63)$$

Moreover, as discussed in [20], the CRB is a tight bound in a scenario of preferable node geometry and high signal to noise ratio (SNR), and thus, is used as the approximation of the estimation covariance exploiting only a snapshot of measurements. As discussed in the description of the PSGD algorithm in Section IV-B, the essential step is to derive

the gradient of the trace of the CRB weighted by a generic weighing matrix Λ w.r.t. the control command $\mathbf{b}_{\mathcal{A}}$, that is

$$\mathbf{c}_{\mathcal{A}} = \nabla_{\mathbf{b}_{\mathcal{A}}} \text{tr}[\Lambda \text{CRB}[\mathbf{x}^{(+)}]]. \quad (64)$$

If the FIM has a full rank, the CRB is expressed as the inverse of the FIM. Subsequently, a closed-form expression of the derivative c_l of the trace of the weighted CRB, $\text{tr}[\Lambda \mathbf{I}_{\mathbf{x}(+)}^{-1}]$ w.r.t. the l th element of $\mathbf{b}_{\mathcal{A}}$, i.e., $b_l = [\mathbf{b}_{\mathcal{A}}]_l$ is derived. Utilizing the derivative chain rule $\partial \mathbf{A}^{-1} = -\mathbf{A}^{-1} \partial \mathbf{A} \mathbf{A}^{-1}$ and the property of the trace $\text{tr}[\mathbf{A}\mathbf{B}] = \text{tr}[\mathbf{B}\mathbf{A}]$, the derivative can be rewritten in the form

$$c_l = \frac{\partial \text{tr}[\Lambda \mathbf{I}_{\mathbf{x}(+)}^{-1}]}{\partial b_l} = -\text{tr} \left[\underbrace{\mathbf{I}_{\mathbf{x}(+)}^{-1} \Lambda \mathbf{I}_{\mathbf{x}(+)}^{-1}}_{\triangleq \mathbf{A}} \frac{\partial \mathbf{I}_{\mathbf{x}(+)}}{\partial b_l} \right]. \quad (65)$$

The expanded closed-form expression of (65) is lengthy, and therefore is stored in Appendix VII. The derivative $\mathbf{c}_{\mathcal{A}}$ of $\text{tr}[\Lambda \mathbf{I}_{\mathbf{x}(+)}^{-1}]$ w.r.t. $\mathbf{b}_{\mathcal{A}}$ is obtained by stacking all c_l , i.e., $\mathbf{c}_{\mathcal{A}} = \text{vec}\{c_l : l = 1, \dots, 2|\mathcal{A}|\}$, which can be used for controller design based on the PSGD introduced in Section IV-B. In practice, the initiated control can be set to zero, that is, $\mathbf{b}_{\mathcal{A}} = \mathbf{0}$, and the current agents' positions are replaced by their estimates. Hence, the gradient is evaluated at the current agents' estimated positions. With the gradient of weighted estimation CRB w.r.t. the control command $\mathbf{b}_{\mathcal{A}}$ being derived, the FI seeking controller can be designed.

D. Bayesian Information Seeking

For the BI seeking, the state $\mathbf{x}^{(+)}$ is considered as a random vector. Not only the predicted snapshot measurements $\tilde{\mathbf{z}}^{(+)}$ but also the historical measurements $\mathbf{z}^{(1:-)}$ are exploited for the state estimation. We focus on full rank cases. Hence, the PCRB, which is a lower bound of the covariance matrix of a Bayesian estimate $\hat{\mathbf{x}}^{(+)}$, is expressed as the inverse of the BIM, denoted as $\mathbf{J}_{\mathbf{x}(+)}$, that is

$$\text{cov}_{\mathbf{x}(+)|\mathbf{z}^{(1:-)}, \tilde{\mathbf{z}}^{(+)}}[\hat{\mathbf{x}}^{(+)}] \succcurlyeq \text{PCRB}[\mathbf{x}^{(+)}] \triangleq \mathbf{J}_{\mathbf{x}(+)}^{-1}. \quad (66)$$

The full rank BIM assumption is valid for swarm navigation in the global coordinate system \mathbb{G} with a sufficient number of beacons. The information about $\mathbf{x}^{(+)}$ in the predicted measurements $\tilde{\mathbf{z}}^{(+)}$ is denoted as $\mathbf{I}_{\mathbf{x}(+)}$, which has a similar expression as the FI in the non-Bayesian case. Unlike the FIM, calculating BIM takes the state's dynamic model (44) into account. With the linear state transition model and the nonlinear observation model both distorted by AWGN, the BIM in (27) simplifies to

$$\mathbf{J}_{\mathbf{x}(+)} = \mathbb{E}_{\mathbf{x}(+)}[\mathbf{I}_{\mathbf{x}(+)}] + \underbrace{(\mathbf{Q}(\mathbf{b}_{\mathcal{A}}) + \mathbf{J}_{\mathbf{x}(-)}^{-1})^{-1}}_{\triangleq \tilde{\mathbf{J}}_{\mathbf{x}(+)}}. \quad (67)$$

The term $\tilde{\mathbf{J}}_{\mathbf{x}(+)}$ is the *a priori* information after the state transition but before obtaining the predicted measurements $\tilde{\mathbf{z}}^{(+)}$. The term $\mathbf{Q}(\mathbf{b}_A)$ is the previously introduced covariance matrix of the state transition noise introduced, which depends on the step size of the individual agent $\|\mathbf{b}_u\|$. A lower bound of the estimation covariance without the predicted measurements $\tilde{\mathbf{z}}^{(+)}$ is obtained by the inverse of $\tilde{\mathbf{J}}_{\mathbf{x}(+)}$, that is,

$$\text{cov}_{\mathbf{x}(+)|\mathbf{z}^{(1:-)}}[\tilde{\mathbf{x}}^{(+)}] \succcurlyeq (\tilde{\mathbf{J}}_{\mathbf{x}(+)})^{-1} \quad (68)$$

which can be used, for example, in stochastic collision avoidance in (51). Similar to the FI seeking control, the essential step of the BI seeking control, both as a cost function and as a constraint, is to derive the gradient of the trace of the PCRB weighted by a generic diagonal weighing matrix $\mathbf{\Lambda}$ w.r.t. the control command \mathbf{b}_A , that is

$$\mathbf{c}_A = \nabla_{\mathbf{b}_A} \text{tr}[\mathbf{\Lambda} \text{PCRB}[\mathbf{x}^{(+)}]] = \nabla_{\mathbf{b}_A} \text{tr}[\mathbf{\Lambda} \mathbf{J}_{\mathbf{x}(+)}^{-1}]. \quad (69)$$

The partial derivative $\nabla_{\mathbf{b}_A} \text{tr}[\mathbf{\Lambda} \mathbf{J}_{\mathbf{x}(+)}^{-1}]$ can be derived similarly as the one for the FI seeking case in Section IV-C. The derivative w.r.t. the l th element of \mathbf{b}_A , i.e., $b_l = [\mathbf{b}_A]_l$ is expressed as

$$\begin{aligned} & \frac{\partial \text{tr}[\mathbf{\Lambda} \mathbf{J}_{\mathbf{x}(+)}^{-1}]}{\partial b_l} \\ &= -\text{tr} \left[\tilde{\mathbf{A}} \frac{\partial \mathbb{E}_{\mathbf{x}(+)}[\mathbf{I}_{\mathbf{x}(+)}]}{\partial b_l} \right] + \frac{\sigma_0^2 b_l}{\|\mathbf{b}_u\|} \text{tr}[\mathbf{B}_{\langle \mathbf{p}_u, \mathbf{p}_u \rangle}] \end{aligned} \quad (70)$$

where

$$\mathbf{B} \triangleq \tilde{\mathbf{J}}_{\mathbf{x}(+)} \tilde{\mathbf{A}} \tilde{\mathbf{J}}_{\mathbf{x}(+)}^{-1}. \quad (71)$$

The term $\mathbf{B}_{\langle \mathbf{p}_u, \mathbf{p}_u \rangle}$ is the 2×2 matrix, truncated from \mathbf{B} at the two rows and two columns with the indices of \mathbf{p}_u from the total state \mathbf{x} . The derivation of (70) is detailed in Appendix C.

In order to evaluate the expectation over $\mathbf{x}^{(+)}$, the *a posteriori* pdf of $\mathbf{x}^{(+)}$ needs to be estimated, which makes the Bayesian controller unattractive for a large-scale swarm [30]. Intensive research has been conducted on the *a posteriori* pdf inference with reduced complexity [27], [97]. This article focuses on the concept of exploiting the position information awareness for swarm formation optimization. Therefore, as suggested in [40, p. 80], we use the value calculated from the estimated state $\hat{\mathbf{x}}^{(+)}$ to replace the expectation without further investigation of Bayesian inference techniques to maintain the low complexity of the swarm controller. The derivative \mathbf{c}_A of $\text{tr}[\mathbf{\Lambda} \mathbf{J}_{\mathbf{x}(+)}^{-1}]$ w.r.t. \mathbf{b}_A can be expressed as $\mathbf{c}_A = \text{vec}\{c_l : l = 1, \dots, 2|\mathcal{A}|\}$ and used for a gradient-based controller similar to the one in Section IV-C.

We can observe that the second term in (70) depends only on the direction of the control vector instead of the

step size. Additionally, it is proportional to the directional vector of the control command. Hence, it does not change the direction of the control commands for each agent, but only reduces their step size. This reduction is due to the step size dependent transition uncertainty defined in (46). The amount of step size reduction differs from agent to agent. With these observations, we can set the initiated control to zero, that is, $\mathbf{b}_A = \mathbf{0}$, to calculate the direction of the gradient from the first term in (70). Then we assume the control vector points into the opposite direction to the gradient to calculate the step size reduction by the second term.

E. Summary of Swarm Control

Similar to the swarm localization in Section III, we summarize the main findings from this section w.r.t. swarm control.

- Swarm control can be formulated as a generic multiobjective optimization problem, with information seeking as either cost function or constraints, and other mission objectives like goal approaching and collision avoidance.
- Weighted CRB and PCRB with mobility models and predicted measurements are utilized for the FI seeking and BI seeking swarm control, respectively.
- Gradients of the weighted CRB and PCRB are derived analytically, allowing the design of a low complexity information seeking swarm controller.

Next, we demonstrate the usage of the self-aware swarm navigation concept via a case study.

V. CASE STUDY: SELF-AWARE SWARM NAVIGATION IN MARS EXPLORATION MISSION

In this section, we conduct simulations to demonstrate self-aware swarm navigation in the Mars exploration mission illustrated in Fig. 1. The RF signals propagating on A2A links use a carrier frequency of $f_c = 5.2$ GHz and a bandwidth of $B_c = 37$ MHz, whereas the ones on S2A links use a carrier frequency of $f_s = 20$ MHz and a bandwidth of $B_s = 1$ kHz. For both RF types, a transmit power of 0 dBm, the free-space pathloss model and an additional noise figure of 15 dB are assumed. All the agents and sources are neither carrier nor symbol synchronized. The symbol delays of the A2A and S2A links and the carrier phases of the S2A links are exploited for swarm navigation. Agents can also measure the gas concentration level at their positions, with the nuisance parameters $b_{\text{gas}} = -1$ and $a_{\text{gas}} = 10^4$. The standard deviations (sdvs) of the observed distance from the different signal models are plotted in Fig. 6. These models account for the limited coverage of the A2A symbol delay observation and of the B2A and S2A the carrier phase observation, due to low SNR and other propagation effects, similar as in [93]. RII with the measurement models can be calculated to derive the joint localization CRB.

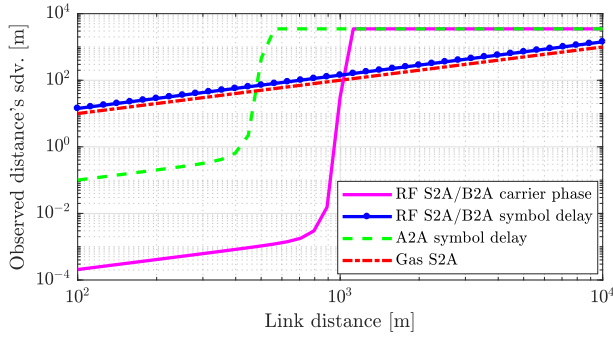


Fig. 6. Standard deviation (sdv) of the observed distance according to the signal models under investigation.

A. Swarm Localization

First, we demonstrate the swarm joint self- and source localization in the considered Mars exploration mission.

A swarm of 30 agents assembles in a predefined formation, connecting the beacons and the gas source. The position CRBs of agents and sources considering different observations are shown in Fig. 7. The beacons, agents, RF sources, and a gas source are illustrated by the blue, green, magenta, and red marker(s), respectively. The effective RF measurement coverage is defined as the link distance, where the observed distance sdvs are smaller than 10 m. The effective RF links are indicated with gray lines. The ellipses in red, blue, and magenta are the 50σ CRB ellipses for nonco-operative (B2A only), co-operative (B2A + A2A) and total (B2A + A2A + S2A) link usage. Very large ellipses are omitted for better visualization.

First, for nonco-operative localization, the red CRB ellipses at the left part of the figure quickly expand in the B2A link direction when an agent is further away from the beacons. This is due to the phase offset between beacons and agents, and coincides with the discovery in (43). Hence, the distance uncertainty dominates the position error when a distance offset type nuisance parameter is unknown. Secondly, by A2A co-operative links, the agent position accuracy improves significantly, which is illustrated by the blue ellipses in the middle of the figure. The uncertainty in this case is mainly on the perpendicular direction of the A2A link. That is because the A2A links are symmetric bidirectional links, where the clock offsets are compensated out in RTT observations. Hence, an A2A link is equivalent to a synchronized ToA link. Last but not least, a further improvement can be obtained by jointly estimating the states of the agents and the sources, which is visible from the total CRB ellipses in magenta at the right part of the figure.

B. Swarm Control

Next, we conduct a case study of the proposed swarm control in the Mars exploration mission.

The system setup in this section is summarized as follows. Initially, agents are randomly located close to the mission base and aim to localize a gas source 4 km away.

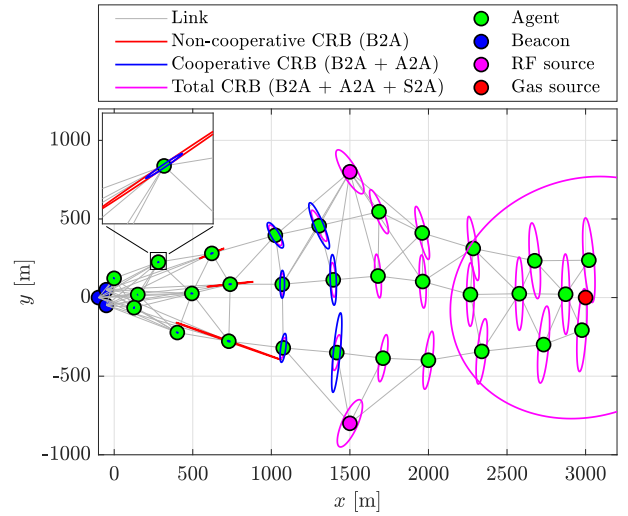


Fig. 7. Swarm exploration scenario with two RF sources, one gas source, and 30 agents. Links are indicated in light gray. Colored ellipses represent the 50σ snapshot position CRB for agents (very large ellipses are omitted) and sources, respectively. The cases of nonco-operative (B2A only), co-operative (B2A + A2A) and total (B2A + A2A + S2A) link usage are shown.

When the goal approaching objective is applied, the estimated gas source position is set as the goal. An agent considers the goal approaching is accomplished if the estimated distance between the goal and itself is smaller than 500 m. A discrete time step model is assumed, where agents apply the routine of move-stop-take measurement-move. Measurements from RF signals, that is, symbol delay and carrier phase with a unit of meters, are generated with the true link distance biased with the clock and carrier offsets and distorted with AWGN with sdvs depicted in Fig. 6. This model is accurate for high SNR [18] with short-to-moderate link distances. For a link with a large distance, the measurement sdv is so large that it leads to an insignificant contribution to localization. This RF measurement implementation allows us to omit the computationally intensive physical layer (PHY) simulation and instead conduct extensive simulations w.r.t. time steps and simulation runs. The gas concentration measurements are directly generated according to (4) and (15). Agents move according to the mobility model described in (44)–(46), with $\sigma_0^2 = 0.1$ m determining the agent's mobility uncertainty. Hence, when an agent aims to move by 10 m, it will suffer from a position noise with variance 1 m^2 . The maximum agent's step size is set to 0.2 m. The collision avoidance constraint is applied in all scenarios, with a minimum tolerated distance of $d_{\min} = 50$ m. The position information seeking objective is applied as constraints for all agents and the maximum tolerated position error is set to $\varepsilon_{\max, l} = 1 \text{ m}^2, l = 1, \dots, L_p$.

When the position information seeking objective and the goal approaching objective are jointly exploited for the cost function, the unconstrained preferable direction

is generated by combining the gradient of the position information seeking objective \mathbf{c}_A^p and the gradient of the goal approaching objective \mathbf{c}_A^g as

$$\tilde{\mathbf{b}}_A \propto -0.4 \frac{\mathbf{c}_A^p}{\|\mathbf{c}_A^p\|} - 0.6 \frac{\mathbf{c}_A^g}{\|\mathbf{c}_A^g\|}. \quad (72)$$

Two weighing matrices are considered for the information seeking cost functions. In the first setup, only gas source position CRB is considered as the cost function, which is explicitly minimized, that is, $\Lambda = \Lambda_{p_{S_{gas}}}$. In the second setup, the information seeking objective is set as the mixture of 10% agents information seeking and 90% gas source information seeking, i.e., $\Lambda = 0.1\Lambda_{p_A} + 0.9\Lambda_{p_{S_{gas}}}$. We aim at demonstrating the proposed information seeking swarm control concept in general, rather than designing a particular controller for certain applications. With the proposed concept, different swarm controllers can be designed according to applications. In order to focus on the control aspect, a centralized EKF is implemented to track the state \mathbf{x} over time steps. EKF is a commonly applied Bayesian tracking algorithm with low complexity, which performs well for small state transition and measurement noise. The algorithm description of the EKF and its decentralization have frequently appeared in literature, for example, in [98], [99, pp. 459 and 473], and are therefore omitted in this article. For a practical implementation of a swarm navigation system, a decentralized tracking algorithm, see [27], [36], [41], [45], and [48], could be preferable.

We first investigate the impacts of the additional RF source and the knowledge of nuisance parameters on the emerging swarm formation. In this setup, the gas source position CRB is exploited solely as the cost function. Then we compare the FI and BI seeking control, where the cost function is composed of the bounds of the swarm and the gas source positions, as well as goal approaching. In this setup, 500 simulation runs have been conducted to obtain statistical results. Different simulation scenarios are summarized in Table 3, with figure index (Fig.), number of agents $|A|$, number of RF sources $|S_{RF}|$, information criterion (Info.), cost functions (Cost), and the knowledge of nuisance parameters (Nui. par.).

We start with the FI seeking control illustrated in Figs. 8 and 9. Only the gas position CRB is considered as cost function. In the first (see Fig. 8) and second (see Fig. 9) cases, the nuisance parameters are assumed to be known. In the other two cases illustrated in Fig. 9, unknown nuisance parameters are assumed. In Figs. 8 and 9, there are no RF sources, while in Figs. 8 and 9, two RF sources are placed in the middle of the field with unknown positions. The gray scale colors on the agent markers represent their position CRBs in logarithm domain. The magenta dashed circles illustrate the carrier phase measurement coverage of the beacons and the RF sources, defined similarly as in Section V-A. The formations with known nuisance parameters spread

Table 3 Swarm Control Setup

Fig.	$ A $	$ S_{RF} $	Info.	Cost	Nui. par.
8a	50	0	FI	$\Lambda_{p_{S_{gas}}}$	known
8b	50	2	FI	$\Lambda_{p_{S_{gas}}}$	known
9a	50	0	FI	$\Lambda_{p_{S_{gas}}}$	unknown
9b	50	2	FI	$\Lambda_{p_{S_{gas}}}$	unknown
10a 11a	20	2	FI	mixture & goal	unknown
10b 11b	20	2	BI	mixture & goal	unknown

out mainly in the direction perpendicular to the gas source direction, aiming at maximizing the tangential swarm aperture toward the gas source and thus improving the source AoA performance. Meantime, the swarm tries to get closer to the source to improve the S2A measurement quality, while fulfilling the maximum agent position CRB constraints. With unknown nuisance parameters, both source AoA and distance estimation prefer a large tangential swarm aperture. The nuisance parameters a_g and b_g act on the gas concentration as scaling and exponent factor, that is, are not additive to the link distance d_{uv} as in (37). Therefore, according to Proposition 1, the source distance information can not only be observed by the tangential swarm aperture, but also by the radial aperture. As a result, the swarm also expands in the horizontal direction. Some agents even move in the opposite direction of the source such that the swarm's radial aperture is maximized, while fulfilling the maximum agent position CRB constraints. The additional RF sources support the swarm in further extending its aperture, even though their state needs to be jointly estimated.

In the second setup, we compare the FI and the BI seeking controls with 500 simulation runs. For both cases, the information seeking objective is set to a mixture of agent and gas source position seeking. We have a look at the emerging formations of the swarm agents together with the absolute position error in a snapshot in Fig. 10, the heat-maps of agents' positions of all time steps and all simulation runs in Fig. 11, and the localization PCRBS and RMSEs of agents, RF sources, and the gas source in Fig. 12. From the snapshot at time step 20 000 [see Fig. 10(b)], we can observe that the swarm controlled by BI seeking behaves more progressive in goal approaching, since the RF sources' positions are precisely estimated with accumulated measurements and are considered as implicit beacons. In comparison, for FI seeking at the same time step [see Fig. 10(a)], the swarm is still well connected to the beacons so that the whole extended network is localizable by a snapshot of measurements. As we are dealing with a very high-dimensional problem, many local minima exist. A consequence is that in each simulation run different agent formations may emerge. In order to

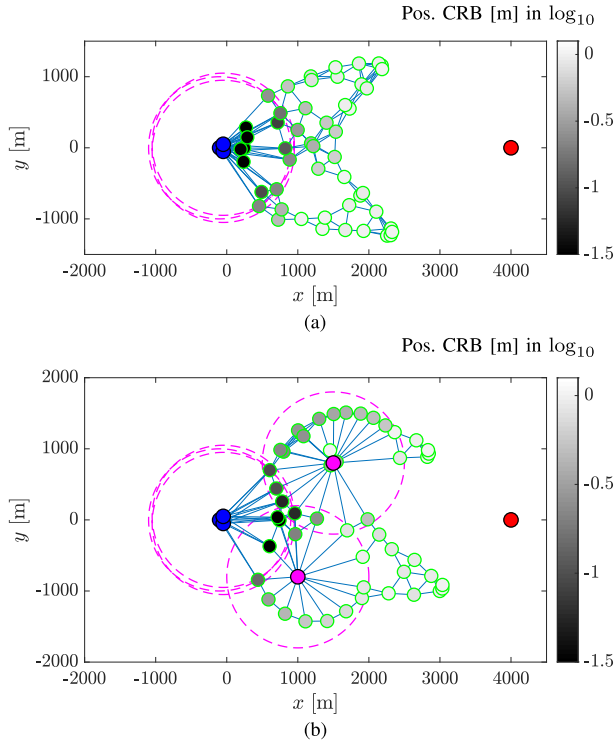


Fig. 8. FI seeking swarm control with known nuisance parameters: Formations at time step 40 000 are plotted. Beacons, RF sources, and a gas source are shown as blue, magenta, and red marker(s), respectively. Agents are shown with green circles filled with gray-scale colors. The colors of the agent circles indicate the value of their position CRBs in logarithm domain. The magenta dashed circles illustrate the carrier phase measurement coverage of the beacons and the RF sources. Blue lines indicate the effective RF links. (a) Without RF source. (b) With two RF sources.

draw conclusions about convergence and formations to be expected in a statistical sense, we produced heat-maps of the entire time span and 500 independent simulation runs (see Fig. 11). Although individual runs are different, one distinct formation for FI seeking control [see Fig. 11(a)], and a significantly different formation for BI seeking control [see Fig. 11(b)] are apparent. We see that, also in a statistical sense, BI seeking control behaves more progressive in goal approaching, while FI seeking control relies on connections to the beacons. Figs. 10 and 12 show that both position PCRBs and RMSEs of agents controlled by BI seeking are larger, but below the maximum tolerated error of $\epsilon_{\max} = 1 \text{ m}^2$ at most of the steps. In exchange, the position PCRb and RMSE of the gas source with BI seeking are an order of magnitude smaller than the ones with FI seeking.

The RMSE curves of EKF in Fig. 12 do not approach the corresponding PCRBs. This can be explained by an estimation bias of the RF sources, introduced by the highly nonlinear measurement model. Despite the bias, EKF provides submeter accuracy for swarm self- and RF source localization, as well as around 10-m accuracy for gas source localization in this challenging scenario. This is considered sufficient for self-aware swarm navigation in the Mars exploration mission under investigation.

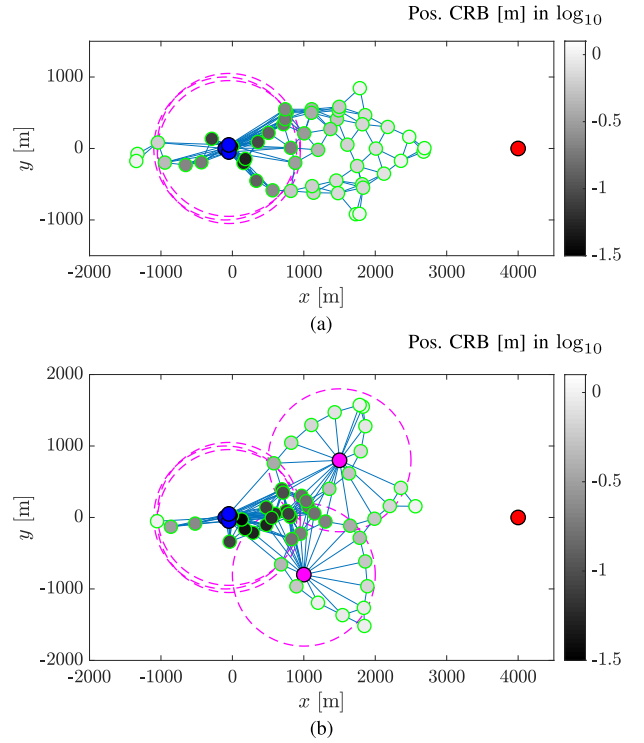


Fig. 9. FI seeking swarm control with unknown nuisance parameters: Similar setup as in Fig. 8 except with unknown nuisance parameters. (a) Without RF source. (b) With two RF sources.

Since the agent position PCRb, a lower bound of the position RMSE, is utilized to formulate the BI seeking constraints, the fulfillment of these constraints cannot be guaranteed. However, we observe from the snapshot in Fig. 12 and the total RMSE curve in Fig. 12 that the BI seeking constraints are mostly fulfilled.

With the case study, we also demonstrate that the proposed information seeking control concept is adaptive according to applications. First, it can be applied as either a cost function or constraints. Second, different weights can be assigned to the positions of individual nodes. Last but not least, either FI or BI can be employed, which leads to different collective behaviors of the swarm.

VI. DISCUSSION

Self-aware swarm navigation is an emerging interdisciplinary topic with proliferated applications not only for exploration missions, but also for, for example, autonomous driving, wireless sensor networks (WSNs) and internet of things (IoT). With this article, we have provided insights into a few aspects of self-aware swarm navigation. A further investigation regarding the following open research topics may lead to fruitful discoveries.

A. System Verification Toward Missions

In order to obtain fundamental understanding of a swarm navigation system, high-level models are widely assumed within this article. To increase the technology

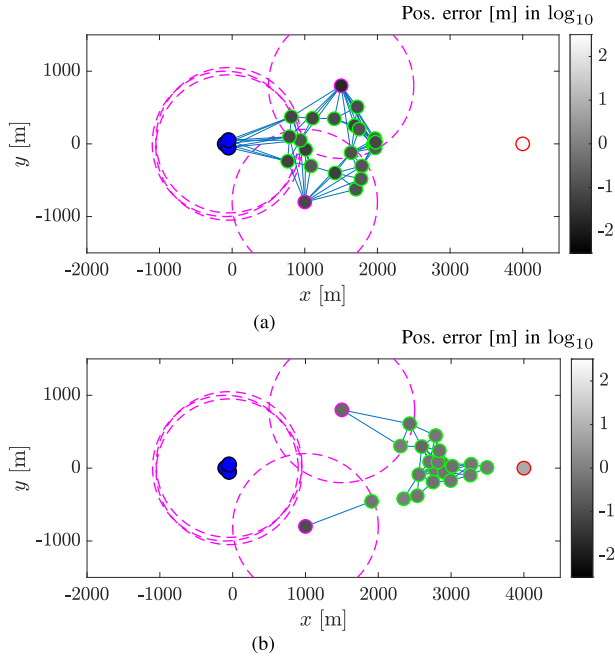


Fig. 10. (a) FI and (b) BI seeking swarm control with unknown nuisance parameters: Formations at time step 20 000 are plotted. Beacons are shown as blue markers. Agents, RF sources, and a gas source are shown as green, magenta, and red circle(s), respectively, filled with gray-scale colors, indicating the value of their absolute position error in logarithm domain.

readiness level (TRL) with the goal of a real mission, advanced models should be applied. Regarding the measurement model, on the one hand, effects like multipath and non-line-of-sight (NLOS) propagation of RF signals [100] and the advection for gas concentration [73] should be taken into account, which might invalidate the radial signal assumption. On the other hand, once the effects are parameterized, a large-scale swarm is suitable for collective estimating these parameters with the discussed SLAX concept. In addition, some effects like the RF multipath and NLOS propagation can be modeled stochastically. These effects may be averaged out by collective observations of a swarm [48]. For the dynamic model of an agent, a high-level way point model is applied in this article. As an extension, a more realistic dynamic model, which also accounts for the low-level controller, should be considered. As discussed earlier, algorithms like ILQR can be applied for information seeking swarm control with an advanced dynamic model. Regarding the control strategy, gradient descent control has the advantage of low complexity. However, it is vulnerable to local minima. For a complex mission, the proposed gradient descent control can be combined with more sophisticated control strategies. After performing simulations with an advanced system model, it is, after all, important to also validate the proposed self-aware swarm navigation system with experiments. As a TRL milestone toward a real mission, a demonstration mission under the framework of the Helmholtz Future Project Autonomous Robotic Networks to Help Modern

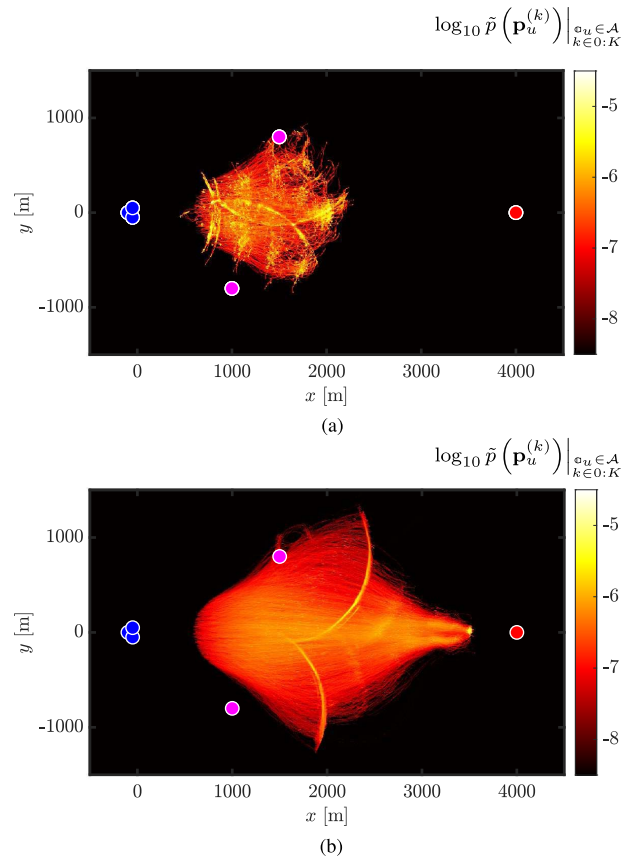


Fig. 11. (a) FI and (b) BI seeking swarm control with unknown nuisance parameters. The empirical pdf heat maps of agents' positions $\tilde{p}(\mathbf{p}_u^{(k)})$ in logarithm are plotted, calculated from all agents, all time steps (0 : K) with K = 20 000 and all 500 simulation runs.

Societies (ARCHES) is planned at a space-analog site on the volcano Mt. Etna, in Sicily, Italy, in June 2021 [101]. The radio-based joint swarm self- and source localization system will be demonstrated in the LOFAR [82] submission.

B. Anchor-Free Navigation

In this article, we have only considered swarm navigation in a global coordinate system. The general concept introduced here can be extended to anchor-free swarm navigation. In that case, agents would need to consent on an internal coordinate system. The fundamental limits of anchor-free localization are addressed in [102] and [103]. Information seeking swarm control for anchor-free applications is discussed preliminarily in [83] and [93], but deserves further investigation.

C. Decentralization

For the information seeking control, full knowledge of the estimated FIM or BIM entities is assumed. The self-aware swarm navigation using a centralized EKF benchmarks the potential performance of a decentralized swarm system. Decentralization is a crucial topic toward the implementation of such a swarm system in reality due

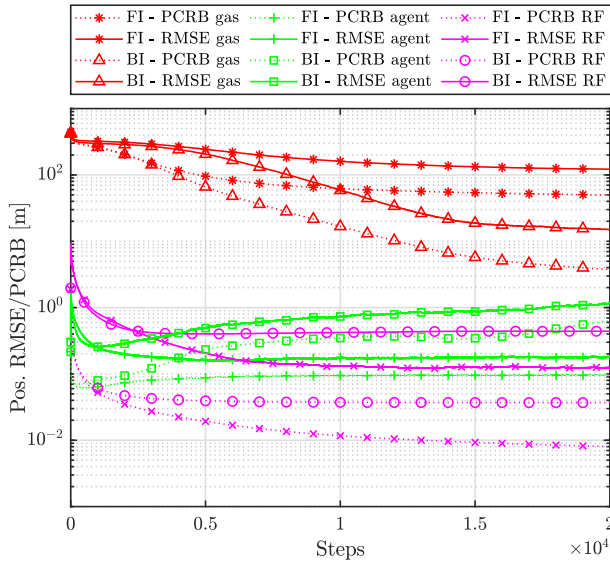


Fig. 12. Information seeking swarm control with unknown nuisance parameters. Position PCRBs and RMSEs of gas source (red), agents (green) and RF sources (magenta), calculated from 500 simulation runs. In 0.4% of the FI seeking runs and 3.2% of the BI seeking runs, the EKF cannot effectively estimate the state, which are considered as outliers and excluded from the RMSE calculation.

to the limited computation and communication capability of individual agents. From the algorithmic perspective, consensus-based decentralized algorithms calculate exactly the same solution as the centralized ones, but at the cost of a large number of iterations. Most of the decentralized localization algorithms in literature like SPAWN only approximate a partition of information at each node, which significantly reduces the complexity. The decentralized localization algorithm proposed in [48] requires low computational power and only few messages to be exchanged among agents. An adequate study on the impacts of decentralization on information seeking control is still missing. From the communication perspective, swarm systems require a specifically designed self-organizing communication protocol [104]. The desynchronization protocol in [105]–[107] is potentially suitable. The emerging time-division multiple access (TDMA) structure from desynchronization guarantees interference-free RF communications and measurements. To sum up, a joint view on swarm communications, localization and control [108] is important for designing a fully decentralized swarm system.

VII. CONCLUSION

With this article, we introduce the concept of self-aware swarm navigation, bridging the fields of swarm localization and swarm control, which have mostly been investigated independently of each other. For the localization perspective, we investigate the generic joint swarm and external source localization problem with the theoretical tools of FI and BI. For a large-scale swarm, compact analytical expressions of the localization CRB are derived, which provide insights on fundamentals of swarm localization. On

this basis, we propose the concept of information seeking swarm control. The swarm becomes aware of the causality between its position and the estimation uncertainty of both its own position and the positions of external sources. This knowledge allows the swarm to autonomously control its formation such that the localization performance of agents and external sources is improved. Thereby, the swarm exhibits collective self-awareness. Investigation of a case-study shows that FI seeking control leads to a more conservative behavior w.r.t. swarm self-localization, whereas BI seeking control is more progressive in terms of goal approaching. The arising swarm formations are well in line with the theory-based intuitions. In conclusion, self-aware swarm navigation is a versatile tool to increase the level of autonomy of extraterrestrial exploration missions. ■

APPENDIX A CONDITION OF NONOBSERVABLE SOURCE DISTANCE

The condition of nonobservable source distance from a 1D swarm collinear to the source is proven as follows:

$$\begin{aligned} \det[\mathbf{I}_{\mathbf{x}_v}] &= 0 \\ \mathbb{E}_{\mathbf{p}_u^p} \left[\iota_{g_{uv}} \left(\frac{\partial g_{uv}}{\partial d_v} \right)^2 \right] \mathbb{E}_{\mathbf{p}_u^p} \left[\iota_{g_{uv}} \left(\frac{\partial g_{uv}}{\partial a_v} \right)^2 \right] \\ - \mathbb{E}_{\mathbf{p}_u^p} \left[\iota_{g_{uv}} \frac{\partial g_{uv}}{\partial d_v} \frac{\partial g_{uv}}{\partial a_v} \right]^2 &= 0 \end{aligned} \quad (73)$$

$$\begin{aligned} \mathbb{E}_{\mathbf{p}_u^p, \mathbf{p}_w^p} \left[\iota_{g_{uv}} \iota_{g_{wv}} \left(\frac{\partial g_{uv}}{\partial d_v} \frac{\partial g_{wv}}{\partial a_v} \right)^2 \right] \\ - \mathbb{E}_{\mathbf{p}_u^p, \mathbf{p}_w^p} \left[\iota_{g_{uv}} \iota_{g_{wv}} \left(\frac{\partial g_{uv}}{\partial d_v} \frac{\partial g_{uv}}{\partial a_v} \right) \left(\frac{\partial g_{wv}}{\partial d_v} \frac{\partial g_{wv}}{\partial a_v} \right) \right] &= 0 \\ \mathbb{E}_{\{\mathbf{p}_u^p: d_u > d_w\}, \mathbf{p}_w^p} \left[\iota_{g_{uv}} \iota_{g_{wv}} \left(\frac{\partial g_{uv}}{\partial a_v} \frac{\partial g_{wv}}{\partial d_v} - \frac{\partial g_{uv}}{\partial d_v} \frac{\partial g_{wv}}{\partial a_v} \right)^2 \right] &= 0 \end{aligned} \quad (74)$$

$$\frac{\partial g_{uv}}{\partial d_v} \frac{\partial g_{wv}}{\partial d_v} = \frac{\partial g_{wv}}{\partial d_v} \frac{\partial g_{uv}}{\partial d_v} \quad \forall u \neq w \quad (75)$$

$$\frac{\partial g_{uv}}{\partial d_v} \frac{\partial g_{uv}}{\partial a_v} = \frac{\partial g_{wv}}{\partial d_v} \frac{\partial g_{wv}}{\partial a_v} \quad \forall u \neq w. \quad (76)$$

It is straightforward to prove that the equality (76) is equivalent to (36).

APPENDIX B PARTIAL DERIVATIVE OF WEIGHTED CRB

The gradient at the l th dimension of \mathbf{c}_A can be written as

$$\begin{aligned} c_l &= \frac{\partial \text{tr}[\mathbf{\Lambda}(\mathbf{I}_x^{(+)})^{-1}]}{\partial b_l} \\ &= -\text{tr} \left[\underbrace{(\mathbf{I}_x^{(+)})^{-1} \mathbf{\Lambda}(\mathbf{I}_x^{(+)})^{-1}}_A \frac{\partial \mathbf{I}_x^{(+)}}{\partial b_l} \right] \end{aligned} \quad (77)$$

$$\begin{aligned}
&= -\text{tr} \left[\sum_{e_{uv} \in \mathcal{E}} \left(\frac{\mathbf{A}_{\langle \mathbf{x}_u, \mathbf{x}_u \rangle} \mathbf{A}_{\langle \mathbf{x}_u, \mathbf{x}_v \rangle}}{\mathbf{A}_{\langle \mathbf{x}_v, \mathbf{x}_u \rangle} \mathbf{A}_{\langle \mathbf{x}_v, \mathbf{x}_v \rangle}} \right) \right. \\
&\quad \left. \times \frac{\partial}{\partial b_l} (\mathbf{I}_{\mathbf{x}_{uv}}^{s_{uv}} + \mathbf{I}_{\mathbf{x}_{uv}}^{s_{uv}}) \right] \\
&\quad - \text{tr} \left[\sum_{e_{uv} \in \mathcal{E}} \mathbf{A}_{\langle \mathbf{x}_u, \mathbf{x}_u \rangle} \frac{\partial}{\partial b_l} \mathbf{I}_{\mathbf{x}_u}^{s_{uv}} \right] \quad (78)
\end{aligned}$$

where $\mathbf{x}_{uv} = \text{vec}\{\mathbf{x}_u, \mathbf{x}_v\}$ and $\mathbf{I}_{\mathbf{x}_c}^{s_{mn}}$ is the information about \mathbf{x}_c contained in the observation of s_{mn} , that is

$$\mathbf{I}_{\mathbf{x}_c}^{s_{mn}} \triangleq \begin{cases} \iota_{mn} \nabla_{\mathbf{x}_c} g_{mn} \nabla_{\mathbf{x}_c}^T g_{mn}, & \text{if } e_{mn} \in \mathcal{E} \\ \mathbf{0}, & \text{otherwise.} \end{cases}$$

A general term in (78) can be expressed analytically as

$$\begin{aligned}
&-\text{tr} \left[\mathbf{A}_{op} \frac{\partial}{\partial b_l} \mathbf{I}_{\mathbf{x}_c}^{s_{mn}} \right] \\
&= -\text{tr} \left[\mathbf{A}_{op} \left(\frac{\partial \nabla_{\mathbf{x}_c} g_{mn}}{\partial b_l} \iota_{mn} \nabla_{\mathbf{x}_c}^T g_{mn} + \nabla_{\mathbf{x}_c} g_{mn} \frac{\partial \iota_{mn}}{\partial b_l} \nabla_{\mathbf{x}_c}^T g_{mn} \right. \right. \\
&\quad \left. \left. + (\nabla_{\mathbf{x}_c} g_{mn}) \iota_{mn} \frac{\partial \nabla_{\mathbf{x}_c}^T g_{mn}}{\partial b_l} \right) \right] \\
&= -\nabla_{\mathbf{x}_c}^T g_{mn} \mathbf{A}_{op} \frac{\partial \nabla_{\mathbf{x}_c} g_{mn}}{\partial b_l} \iota_{mn} \\
&\quad - \nabla_{\mathbf{x}_c}^T g_{mn} \mathbf{A}_{op} \nabla_{\mathbf{x}_c} g_{mn} \frac{\partial \iota_{mn}}{\partial b_l} \\
&\quad - \frac{\partial \nabla_{\mathbf{x}_c}^T g_{mn}}{\partial b_l} \mathbf{A}_{op} (\nabla_{\mathbf{x}_c} g_{mn}) \iota_{mn}
\end{aligned}$$

$$\begin{aligned}
&= -\frac{\partial \nabla_{\mathbf{x}_c}^T g_{mn}}{\partial b_l} (\mathbf{A}_{op} + \mathbf{A}_{op}^T) \nabla_{\mathbf{x}_c} g_{mn} \iota_{mn} \\
&\quad - \nabla_{\mathbf{x}_c}^T g_{mn} \mathbf{A}_{op} \nabla_{\mathbf{x}_c} g_{mn} \frac{\partial \iota_{mn}}{\partial b_l}. \quad (79)
\end{aligned}$$

The partial derivative c_l can be formulated analytically by combining (78) and (79).

APPENDIX C PARTIAL DERIVATIVE OF WEIGHTED PCRB

$$\begin{aligned}
&\frac{\partial \text{tr} [\mathbf{A} \mathbf{J}_{\mathbf{x}(+)}^{-1}]}{\partial b_l} \\
&= -\text{tr} \left[\underbrace{\mathbf{J}_{\mathbf{x}(+)}^{-1} \mathbf{A} \mathbf{J}_{\mathbf{x}(+)}^{-1}}_{\triangleq \tilde{\mathbf{A}}} \frac{\partial \mathbf{J}_{\mathbf{x}(+)}^{-1}}{\partial b_l} \right] \quad (80)
\end{aligned}$$

$$= -\text{tr} \left[\tilde{\mathbf{A}} \left(\frac{\partial \mathbb{E}_{\mathbf{x}(+)} [\mathbf{I}_{\mathbf{x}(+)}]}{\partial b_l} + \frac{\partial \tilde{\mathbf{J}}_{\mathbf{x}(+)}}{\partial b_l} \right) \right] \quad (81)$$

$$= -\text{tr} \left[\tilde{\mathbf{A}} \frac{\partial \mathbb{E}_{\mathbf{x}(+)} [\mathbf{I}_{\mathbf{x}(+)}]}{\partial b_l} \right] + \text{tr} \left[\mathbf{B} \frac{\partial \mathbf{Q}(\mathbf{b}_A)}{\partial b_l} \right]. \quad (82)$$

The expression in (70) can be obtained readily from (82).

Acknowledgment

The authors would like to express their gratitude to the editors and the anonymous reviewers for their careful reading of this article and helpful suggestions.

REFERENCES

- [1] M. Ballerini et al., "Interaction ruling animal collective behavior depends on topological rather than metric distance: Evidence from a field study," *Proc. Nat. Acad. Sci. USA*, vol. 105, no. 4, pp. 1232–1237, Jan. 2008.
- [2] C. W. Reynolds, "Flocks, herds and schools: A distributed behavioral model," in *Proc. 14th Annu. Conf. Comput. Graph. Interact. Techn. (SIGGRAPH)*. New York, NY, USA: ACM, 1987, pp. 25–34.
- [3] S. Johnson, *Emergence: The Connected Lives of Ants, Brains, Cities, and Software* (Touchstone Book). New York, NY, USA: Simon and Schuster, 2001.
- [4] M. Moussaid, S. Garnier, G. Theraulaz, and D. Helbing, "Collective information processing and pattern formation in swarms, flocks, and crowds," *Topics Cognit. Sci.*, vol. 1, no. 3, pp. 469–497, Jul. 2009.
- [5] M. G. Hinchey, R. Sterritt, and C. Rouff, "Swarms and swarm intelligence," *Computer*, vol. 40, no. 4, pp. 111–113, Apr. 2007.
- [6] S.-J. Chung, A. A. Paranjape, P. Dames, S. Shen, and V. Kumar, "A survey on aerial swarm robotics," *IEEE Trans. Robot.*, vol. 34, no. 4, pp. 837–855, Aug. 2018.
- [7] H. Hamann, *Swarm Robotics: A Formal Approach*, 1st ed. Basel, Switzerland: Springer, 2018.
- [8] S. Li et al., "Particle robotics based on statistical mechanics of loosely coupled components," *Nature*, vol. 567, no. 7748, pp. 361–365, Mar. 2019.
- [9] M. Bernard, K. Kondak, I. Maza, and A. Ollero, "Autonomous transportation and deployment with aerial robots for search and rescue missions," *J. Field Robot.*, vol. 28, no. 6, pp. 914–931, Nov. 2011.
- [10] M. Dunbabin and L. Marques, "Robots for environmental monitoring: Significant advancements and applications," *IEEE Robot. Autom. Mag.*, vol. 19, no. 1, pp. 24–39, Mar. 2012.
- [11] A. Seeni, B. Schfer, and G. Hirzinger, "Robot mobility systems for planetary surface exploration—State-of-the-art and future outlook: A literature survey," in *Aerospace Technologies Advancements*, T. T. Arif, Ed. London, U.K.: InTech, Jan. 2010, pp. 189–208.
- [12] A. Wedler et al., "From single autonomous robots toward cooperative robotic interactions for future planetary exploration missions," in *Proc. Int. Astron. Congr. (IAC)*. Bremen, Germany: International Astronautical Federation, Oct. 2018, pp. 1–8.
- [13] P. van Vugt, A. Meijerink, and M. Bentum, "Calibration of the OLFAR space-based radio telescope using a weighted alternating least squares approach," in *Proc. IEEE Aerosp. Conf.*, Mar. 2017, pp. 1–11.
- [14] W. Truszkowski, M. Hinchey, J. Rash, and C. Rouff, "NASA's swarm missions: The challenge of building autonomous software," *IT Prof.*, vol. 6, no. 5, pp. 47–52, Sep. 2004.
- [15] M. Bajracharya, M. W. Maimone, and D. Helmick, "Autonomy for mars rovers: Past, present, and future," *Computer*, vol. 41, no. 12, pp. 44–50, Dec. 2008.
- [16] S. Engelen, E. Gill, and C. Verhoeven, "On the reliability, availability, and throughput of satellite swarms," *IEEE Trans. Aerosp. Electron. Syst.*, vol. 50, no. 2, pp. 1027–1037, Apr. 2014.
- [17] N. Patwari, J. N. Ash, S. Kyperountas, A. O. Hero, R. L. Moses, and N. S. Correal, "Locating the nodes: Cooperative localization in wireless sensor networks," *IEEE Signal Process. Mag.*, vol. 22, no. 4, pp. 54–69, Jul. 2005.
- [18] D. Dardari, A. Conti, U. Ferner, A. Giorgetti, and M. Z. Win, "Ranging with ultrawide bandwidth signals in multipath environments," *Proc. IEEE*, vol. 97, no. 2, pp. 404–426, Feb. 2009.
- [19] Y. Shen, S. Mazuelas, and M. Z. Win, "Network navigation: Theory and interpretation," *IEEE J. Sel. Areas Commun.*, vol. 30, no. 9, pp. 1823–1834, Oct. 2012.
- [20] M. Z. Win, Y. Shen, and W. Dai, "A theoretical foundation of network localization and navigation," *Proc. IEEE*, vol. 106, no. 7, pp. 1136–1165, Jul. 2018.
- [21] M. Cobos, F. Antonacci, A. Alexandridis, A. Mouchtaris, and B. Lee, "A survey of sound source localization methods in wireless acoustic sensor networks," *Wireless Commun. Mobile Comput.*, vol. 2017, pp. 1–24, 2017.
- [22] C. Rascon and I. Meza, "Localization of sound sources in robotics: A review," *Robot. Autom. Syst.*, vol. 96, pp. 184–210, Oct. 2017.
- [23] C. Nicol, A. Ellery, B. Lynch, E. Cloutis, and G. de Croon, "Martian methane plume models for defining mars rover methane source search strategies," *Int. J. Astrobiol.*, vol. 17, no. 3, pp. 228–238, Jul. 2018.
- [24] N. Poiata, C. Satriano, J.-P. Vilotte, P. Bernard, and K. Obara, "Multiband array detection and location of seismic sources recorded by dense seismic networks," *Geophys. J. Int.*, vol. 205, no. 3, pp. 1548–1573, Jun. 2016.
- [25] R. M. Murray, "Recent research in cooperative control of multivehicle systems," *J. Dyn. Syst., Meas., Control*, vol. 129, no. 5, pp. 571–583, Sep. 2007.
- [26] M. Viberg, "Introduction to array processing," in *Academic Press Library in Signal Processing*, vol. 3, A. M. Zoubir, M. Viberg, R. Chellappa, and S. Theodoridis, Eds. Boston, MA, USA: Elsevier, 2014, ch. 11, pp. 463–502.

- [27] H. Wymeersch, J. Lien, and M. Win, "Cooperative localization in wireless networks," *Proc. IEEE*, vol. 97, no. 2, pp. 427–450, Feb. 2009.
- [28] H. Naseri and V. Koivunen, "Cooperative simultaneous localization and mapping by exploiting multipath propagation," *IEEE Trans. Signal Process.*, vol. 65, no. 1, pp. 200–211, Jan. 2017.
- [29] C. Taylor, A. Rahimi, J. Bachrach, H. Shrobe, and A. Grue, "Simultaneous localization, calibration, and tracking in an ad hoc sensor network," in *Proc. 5th Int. Conf. Inf. Process. Sensor Netw. (IPSN)*, Apr. 2006, pp. 27–33.
- [30] F. Meyer, H. Wymeersch, M. Frohle, and F. Hlawatsch, "Distributed estimation with information-seeking control in agent networks," *IEEE J. Sel. Areas Commun.*, vol. 33, no. 11, pp. 2439–2456, Nov. 2015.
- [31] B. Ertzinger, F. Meyer, F. Hlawatsch, A. Springer, and H. Wymeersch, "Cooperative simultaneous localization and synchronization in mobile agent networks," *IEEE Trans. Signal Process.*, vol. 65, no. 14, pp. 3587–3602, Jul. 2017.
- [32] J. Aspnes et al., "A theory of network localization," *IEEE Trans. Mobile Comput.*, vol. 5, no. 12, pp. 1663–1678, Dec. 2006.
- [33] S. M. Kay, *Fundamentals of Statistical Processing, Volume I: Estimation Theory*, 1st ed. Englewood Cliffs, NJ, USA: Prentice-Hall, 1993.
- [34] Y. Shen, H. Wymeersch, and M. Z. Win, "Fundamental limits of wideband Localization—Part II: Cooperative networks," *IEEE Trans. Inf. Theory*, vol. 56, no. 10, pp. 4981–5000, Oct. 2010.
- [35] J. P. Delmas, M. N. El Korso, H. Gazzah, and M. Castella, "CRB analysis of planar antenna arrays for optimizing near-field source localization," *Signal Process.*, vol. 127, pp. 117–134, Oct. 2016.
- [36] S. Zhang, T. Jost, R. Pohlmann, A. Dammann, D. Shutin, and P. A. Hoehner, "Spherical wave positioning based on curvature of arrival by an antenna array," *IEEE Wireless Commun. Lett.*, vol. 8, no. 2, pp. 504–507, Apr. 2019.
- [37] S. Zhang, R. Pohlmann, and A. Dammann, "Heterogeneous network localization with a distributed phased array composed of cooperative vehicles," in *Proc. 27th Eur. Signal Process. Conf. (EUSIPCO)*, Sep. 2019, pp. 1–5.
- [38] H. L. Van Trees, *Optimum Array Processing: Part IV of Detection, Estimation and Modulation Theory/Harry L. Van Trees*, no. 4. New York, NY, USA: Wiley, 2002.
- [39] P. Tichavsky, C. H. Muravchik, and A. Nehorai, "Posterior cramer-rao bounds for discrete-time nonlinear filtering," *IEEE Trans. Signal Process.*, vol. 46, no. 5, pp. 1386–1396, May 1998.
- [40] H. L. V. Trees and K. L. Bell, *Bayesian Bounds for Parameter Estimation and Nonlinear Filtering/Tracking*. Hoboken, NJ, USA: Wiley, 2007.
- [41] R. M. Buehrer, H. Wymeersch, and R. M. Vaghefi, "Collaborative sensor network localization: Algorithms and practical issues," *Proc. IEEE*, vol. 106, no. 6, pp. 1089–1114, Jun. 2018.
- [42] Y. Zhu, A. Jiang, and H. K. Kwan, "ADMM-based sensor network localization using low-rank approximation," *IEEE Sensors J.*, vol. 18, no. 20, pp. 8463–8471, Oct. 2018.
- [43] S. Safavi, U. A. Khan, S. Kar, and J. M. F. Moura, "Distributed localization: A linear theory," *Proc. IEEE*, vol. 106, no. 7, pp. 1204–1223, Jul. 2018.
- [44] A. T. Ihler, J. W. Fisher, R. L. Moses, and A. S. Willsky, "Nonparametric belief propagation for self-localization of sensor networks," *IEEE J. Sel. Areas Commun.*, vol. 23, no. 4, pp. 809–819, Apr. 2005.
- [45] S. I. Roumeliotis and G. A. Bekey, "Distributed multirobot localization," *IEEE Trans. Robot. Autom.*, vol. 18, no. 5, pp. 781–795, Oct. 2002.
- [46] G. Mao, B. Fidan, and B. D. O. Anderson, "Wireless sensor network localization techniques," *Comput. Netw.*, vol. 51, no. 10, pp. 2529–2553, Jul. 2007.
- [47] P. Closas and A. Gusi-Amigo, "Direct position estimation of GNSS receivers: Analyzing main results, architectures, enhancements, and challenges," *IEEE Signal Process. Mag.*, vol. 34, no. 5, pp. 72–84, Sep. 2017.
- [48] S. Zhang et al., "Distributed direct localization suitable for dense networks," *IEEE Trans. Aerosp. Electron. Syst.*, vol. 56, no. 2, pp. 1209–1227, Apr. 2020.
- [49] A. Conti, S. Mazuelas, S. Bartoletti, W. C. Lindsey, and M. Z. Win, "Soft information for localization-of-things," *Proc. IEEE*, vol. 107, no. 11, pp. 2240–2264, Nov. 2019.
- [50] P. Biswas and Y. Ye, "Semidefinite programming for ad hoc wireless sensor network localization," in *Proc. 3rd Int. Symp. Inf. Process. Sensor Netw. (IPSN)*, Apr. 2004, pp. 46–54.
- [51] V. Fox, J. Hightower, L. Liao, D. Schulz, and G. Borriello, "Bayesian filtering for location estimation," *IEEE Perv. Comput.*, vol. 2, no. 3, pp. 24–33, Jul. 2003.
- [52] M. S. Arulampalam, S. Maskell, N. Gordon, and T. Clapp, "A tutorial on particle filters for online nonlinear/non-Gaussian Bayesian tracking," *IEEE Trans. Signal Process.*, vol. 50, no. 2, pp. 174–188, Feb. 2002.
- [53] O. Hlinka, F. Hlawatsch, and P. M. Djuric, "Distributed particle filtering in agent networks: A survey, classification, and comparison," *IEEE Signal Process. Mag.*, vol. 30, no. 1, pp. 61–81, Jan. 2013.
- [54] B. Cakmak, D. N. Urup, F. Meyer, T. Pedersen, B. H. Fleury, and F. Hlawatsch, "Cooperative localization for mobile networks: A distributed belief propagation—mean field message passing algorithm," *IEEE Signal Process. Lett.*, vol. 23, no. 6, pp. 828–832, Jun. 2016.
- [55] K.-K. Oh, M.-C. Park, and H.-S. Ahn, "A survey of multi-agent formation control," *Automatica*, vol. 53, pp. 424–440, Mar. 2015.
- [56] J. Shamma, *Cooperative Control of Distributed Multi-Agent Systems*. New York, NY, USA: Wiley, 2008.
- [57] W. Ren and Y. Cao, *Distributed Coordination of Multi-Agent Networks Emergent Problems, Models, and Issues*. Basel, Switzerland: Springer, Nov. 2010.
- [58] W. Yu, G. Wen, G. Chen, and J. Cao, *Distributed Cooperative Control of Multi-Agent Systems*. Hoboken, NJ, USA: Wiley, 2017.
- [59] R. Olfati-Saber, "Flocking for multi-agent dynamic systems: Algorithms and theory," *IEEE Trans. Autom. Control*, vol. 51, no. 3, pp. 401–420, Mar. 2006.
- [60] K.-K. Oh and H.-S. Ahn, "Formation control of mobile agents based on distributed position estimation," *IEEE Trans. Autom. Control*, vol. 58, no. 3, pp. 737–742, Mar. 2013.
- [61] Y. Cai and Y. Shen, "An integrated localization and control framework for multi-agent formation," *IEEE Trans. Signal Process.*, vol. 67, no. 7, pp. 1941–1956, Apr. 2019.
- [62] M. Ye, B. D. O. Anderson, and C. Yu, "Bearing-only measurement self-localization, velocity consensus and formation control," *IEEE Trans. Aerosp. Electron. Syst.*, vol. 53, no. 2, pp. 575–586, Apr. 2017.
- [63] Y. Kim, G. Zhu, and J. Hu, "Optimizing formation rigidity under connectivity constraints," in *Proc. 49th IEEE Conf. Decision Control (CDC)*, Dec. 2010, pp. 6590–6595.
- [64] F. Morbidi and G. L. Mariottini, "Active target tracking and cooperative localization for teams of aerial vehicles," *IEEE Trans. Control Syst. Technol.*, vol. 21, no. 5, pp. 1694–1707, Sep. 2013.
- [65] U. Neisser, "The roots of self-knowledge: Perceiving self, it, and thou," *Ann. New York Acad. Sci.*, vol. 818, no. 1, pp. 19–33, Jun. 1997.
- [66] D. Hofstadter, *I Am a Strange Loop*. New York, NY, USA: Basic Books, 2007.
- [67] P. R. Lewis, M. Platzner, B. Rinner, J. Trresen, and X. Yao, *Self-Aware Computing Systems: An Engineering Approach*, 1st ed. Basel, Switzerland: Springer, 2016.
- [68] S. K. Mitter, "Filtering and stochastic control: A historical perspective," *IEEE Control Syst.*, vol. 16, no. 3, pp. 67–76, Jun. 1996.
- [69] P. R. Lewis et al., "Architectural aspects of self-aware and self-expressive computing systems: From psychology to engineering," *Computer*, vol. 48, no. 8, pp. 62–70, Aug. 2015.
- [70] B. Ristic, S. Arulampalam, and N. Gordon, *Beyond the Kalman Filter: Particle Filters for Tracking Applications*. Norwood, MA, USA: Artech House, 2004.
- [71] S. Zhang, R. Raulefs, A. Dammann, and S. Sand, "System-level performance analysis for Bayesian cooperative positioning: From global to local," in *Proc. Int. Conf. Indoor Positioning Indoor Navigat.*, Oct. 2013, pp. 1–10.
- [72] S. Mazuelas et al., "Robust indoor positioning provided by real-time RSSI values in unmodified WLAN networks," *IEEE J. Sel. Topics Signal Process.*, vol. 3, no. 5, pp. 821–831, Oct. 2009.
- [73] T. Wiedemann, D. Shutin, and A. J. Lilienthal, "Model-based gas source localization strategy for a cooperative multi-robot system—A probabilistic approach and experimental validation incorporating physical knowledge and model uncertainties," *Robot. Autonom. Syst.*, vol. 118, pp. 66–79, Aug. 2019.
- [74] R. Pohlmann, S. A. Almasri, S. Zhang, T. Jost, A. Dammann, and P. A. Hoehner, "On the potential of multi-mode antennas for direction-of-arrival estimation," *IEEE Trans. Antennas Propag.*, vol. 67, no. 5, pp. 3374–3386, May 2019.
- [75] S. Alkubti Almasri, R. Pohlmann, N. Doose, P. A. Hoehner, and A. Dammann, "Modeling aspects of planar multi-mode antennas for direction-of-arrival estimation," *IEEE Sensors J.*, vol. 19, no. 12, pp. 4585–4597, Jun. 2019.
- [76] I. Guvenç and C.-C. Chong, "A survey on TOA based wireless localization and NLOS mitigation techniques," *IEEE Commun. Surveys Tuts.*, vol. 11, no. 3, pp. 107–124, 3rd Quart., 2009.
- [77] E. Staudinger, S. Zhang, and A. Dammann, "Cramer-rao lower bound for round-trip delay ranging with subcarrier-interleaved OFDMA," *IEEE Trans. Aerosp. Electron. Syst.*, vol. 52, no. 6, pp. 2961–2972, Dec. 2016.
- [78] J. J. Caffery, *Wireless Location in CDMA Cellular Radio Systems*. Norwell, MA, USA: Kluwer, 1999.
- [79] J. G. Proakis and M. Salehi, *Digital Communications*, 5th ed. Boston, MA, USA: McGraw-Hill, 2008.
- [80] H. Minn, V. K. Bhargava, and K. B. Letaief, "A robust timing and frequency synchronization for OFDM systems," *IEEE Trans. Wireless Commun.*, vol. 24, no. 5, pp. 822–839, May 2003.
- [81] G. B. Taylor, "The long wavelength array," *Proc. Int. Astronomical Union*, vol. 2, no. 14, pp. 388–389, Aug. 2006.
- [82] H. R. Butcher, "LOFAR: First of a new generation of radio telescopes," *Proc. SPIE*, vol. 5489, pp. 537–544, Sep. 2004.
- [83] S. Zhang, R. Raulefs, and A. Dammann, "Location information driven formation control for swarm return-to-base application," in *Proc. 24th Eur. Signal Process. Conf. (EUSIPCO)*, Aug. 2016, pp. 758–763.
- [84] J. Crank and E. Crank, *The Mathematics of Diffusion* (Oxford Science Publications). Oxford, U.K.: Clarendon, 1979.
- [85] H. L. Van Trees, *Detection, Estimation, and Linear Modulation Theory*. Hoboken, NJ, USA: Wiley, 2002.
- [86] H. V. Poor, *An Introduction to Signal Detection and Estimation*. New York, NY, USA: Springer, 1994.
- [87] Y. Shen and M. Z. Win, "Fundamental limits of wideband Localization—Part I: A general framework," *IEEE Trans. Inf. Theory*, vol. 56, no. 10, pp. 4956–4980, Oct. 2010.
- [88] B. Friedlander, "Direction finding using an interpolated array," in *Proc. Int. Conf. Acoust., Speech, Signal Process.*, vol. 5, Apr. 1990, pp. 2951–2954.
- [89] T. E. Tuncer and B. Friedlander, *Classical and Modern Direction-of-Arrival Estimation*. Boston, MA, USA: Academic, 2009.
- [90] M. Haardt, M. Pesavento, F. Roemer, and M. N. E. Korso, "Subspace methods and exploitation of special array structures," in

- Academic Press Library in Signal Processing*, vol. 3, A. M. Zoubir, M. Viberg, R. Chellappa, and S. Theodoridis, Eds. Amsterdam, The Netherlands: Elsevier, 2014, pp. 651–717.
- [91] K. Meyberg and P. Vachenauer, *Höhere Mathematik 2: Differentialgleichungen, Funktionentheorie, Fourier-Analyse, Variationsrechnung*. Berlin, Germany: Springer, 1991.
- [92] J. Chen, W. Zhan, and M. Tomizuka, “Autonomous driving motion planning with constrained iterative LQR,” *IEEE Trans. Intell. Vehicles*, vol. 4, no. 2, pp. 244–254, Jun. 2019.
- [93] S. Zhang, M. Frohle, H. Wymeersch, A. Dammann, and R. Raulefs, “Location-aware formation control in swarm navigation,” in *Proc. IEEE Globecom Workshops (GC Wkshps)*, Dec. 2015, pp. 1–6.
- [94] X. Chen and K. Zhou, “On the probabilistic characterization of model uncertainty and robustness,” in *Proc. 36th IEEE Conf. Decision Control*, vol. 4, Dec. 1997, pp. 3816–3821.
- [95] R. T. Marler and J. S. Arora, “Survey of multi-objective optimization methods for engineering,” *Struct. Multidisciplinary Optim.*, vol. 26, no. 6, pp. 369–395, Apr. 2004.
- [96] R. T. Haftka and Z. Gürdal, *Elements of Structural Optimization*. Springer, 1984.
- [97] F. Meyer, O. Hlinka, and F. Hlawatsch, “Sigma point belief propagation,” *IEEE Signal Process. Lett.*, vol. 21, no. 2, pp. 145–149, Feb. 2014.
- [98] G. Minkler and J. Minkler, *Theory and Application of Kalman Filtering*. Palm Bay, FL, USA: Magellan Book Company, 1993.
- [99] S. I. Roumeliotis and G. A. Bekey, “Collective localization: A distributed Kalman filter approach to localization of groups of mobile robots,” in *Proc. IEEE Int. Conf. Robot. Autom. Symp. Millennium Conf. (ICRA)*, vol. 3, Apr. 2000, pp. 2958–2965.
- [100] J. Karedal et al., “A geometry-based stochastic MIMO model for vehicle-to-vehicle communications,” *IEEE Trans. Wireless Commun.*, vol. 8, no. 7, pp. 3646–3657, Jul. 2009.
- [101] M. J. Schuster et al., “The ARCHES moon-analogue demonstration mission: Towards teams of autonomous robots for collaborative scientific sampling in lunar environments,” in *Proc. 8th Eur. Lunar Symp.*, Padua, Italy, May 2020, pp. 1–2.
- [102] J. N. Ash and R. L. Moses, “On the relative and absolute positioning errors in self-localization systems,” *IEEE Trans. Signal Process.*, vol. 56, no. 11, pp. 5668–5679, Nov. 2008.
- [103] D. C. Popescu, M. Hedley, and T. Sathyan, “Posterior Cramér–Rao bound for anchorless tracking,” *IEEE Signal Process. Lett.*, vol. 20, no. 12, pp. 1183–1186, Dec. 2013.
- [104] T. Andre et al., “Application-driven design of aerial communication networks,” *IEEE Commun. Mag.*, vol. 52, no. 5, pp. 129–137, May 2014.
- [105] J. Degeys, I. Rose, A. Patel, and R. Nagpal, “DESYNC: Self-organizing desynchronization and TDMA on wireless sensor networks,” in *Proc. 6th Int. Symp. Inf. Process. Sensor Netw.*, Apr. 2007, pp. 11–20.
- [106] D. Buranapanichkit, N. Deligiannis, and Y. Andreopoulos, “Convergence of desynchronization primitives in wireless sensor networks: A stochastic modeling approach,” *IEEE Trans. Signal Process.*, vol. 63, no. 1, pp. 221–233, Jan. 2015.
- [107] S. Zhang, S. Sand, R. Raulefs, and E. Staudinger, “Self-organized hybrid channel access method for an interleaved RTD-based swarm navigation system,” in *Proc. 10th Workshop Positioning, Navigat. Commun. (WPNC)*, Mar. 2013, pp. 1–6.
- [108] R. Hult, G. R. Campos, E. Steinmetz, L. Hammarstrand, P. Falcone, and H. Wymeersch, “Coordination of cooperative autonomous vehicles: Toward safer and more efficient road transportation,” *IEEE Signal Process. Mag.*, vol. 33, no. 6, pp. 74–84, Nov. 2016.

ABOUT THE AUTHORS

Siwei Zhang (Member, IEEE) received the B.Sc. degree in electrical engineering from Zhejiang University, Hangzhou, China, in 2009, and the M.Sc. degree in communication engineering from the Technical University of Munich, Munich, Germany, in 2011.

In 2012, he joined the Institute of Communications and Navigation, German Aerospace Center (DLR), Wessling, Germany, as a Research Staff Member. His research interests include cooperative positioning and swarm navigation.



Thomas Wiedemann (Member, IEEE) received the bachelor's and master's degrees from the Faculty of Mechanical Engineering, Technical University of Munich, Munich, Germany, in 2012 and 2014, respectively. He is currently pursuing the Ph.D. degree with the AASS Research Center, Örebro University, Örebro, Sweden, with a focus on exploration strategies for multirobot systems and incorporation domain knowledge for robotic gas source localization.



Since 2014, he has been a Scientist with the Institute of Communications and Navigation, German Aerospace Center (DLR), Wessling, Germany, where he is currently working with the Swarm Exploration Research Group. His research interests include machine learning for signal processing, distributed algorithms, and numerical methods for fluid dynamics.

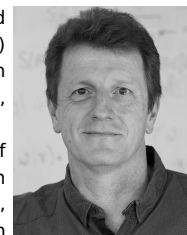
Robert Pöhlmann (Member, IEEE) received the B.Sc. and M.Sc. degrees in electrical engineering and information technology from the Technical University of Munich (TUM), Munich, Germany, in 2014 and 2016, respectively.

In 2013, he joined the Institute of Communications and Navigation, German Aerospace Center (DLR), Wessling, Germany, as a Student Trainee, where he became a Research Staff Member in 2016. His current research interests are in the area of statistical signal processing for multiantenna systems and cooperative localization.



Armin Dammann (Member, IEEE) received the Dipl.Ing. (M.Sc.) and Dr.Ing. (Ph.D.) degrees in electrical engineering from the University of Ulm, Ulm, Germany, in 1997 and 2005, respectively.

In 1997, he joined the Institute of Communications and Navigation, German Aerospace Center (DLR), Cologne, Germany, as a Research Staff Member, where he has been the Head of the Mobile Radio Transmission Research Group since 2005. He is currently a Lecturer with the Technical University of Munich, Munich, Germany, for the Robot and Swarm Navigation. His research interests and activities include signal design and signal processing for terrestrial wireless communications and navigation systems. In these fields, he has been active in several EU-projects, such as WINNER, WHERE, and WHERE2.



Henk Wymeersch (Senior Member, IEEE) received the Ph.D. degree in electrical engineering/applied sciences from Ghent University, Ghent, Belgium, in 2005.

From 2005 to 2009, he was a Postdoctoral Researcher with the Laboratory for Information and Decision Systems, Massachusetts Institute of Technology, Cambridge, MA, USA. He is currently a Professor of communication systems with the Department of Electrical Engineering, Chalmers University of Technology, Gothenburg, Sweden. He is also a Distinguished Research Associate with the Eindhoven University of Technology, Eindhoven, The Netherlands. His current research interest includes the convergence of communication and sensing, in a 5G and beyond 5G context.

Dr. Wymeersch served as an Associate Editor for the IEEE COMMUNICATION LETTERS from 2009 to 2013 and the IEEE TRANSACTIONS ON COMMUNICATIONS from 2016 to 2018. He has been serving as an Associate Editor for the IEEE TRANSACTIONS ON WIRELESS COMMUNICATIONS since 2013. From 2019 to 2021, he is also an IEEE Distinguished Lecturer with the Vehicular Technology Society.



Peter Adam Hoeher (Fellow, IEEE) received the Dipl.Ing. (M.Sc.) degree in electrical engineering from RWTH Aachen University, Aachen, Germany, in 1986, and the Dr.Ing. (Ph.D.) degree in electrical engineering from the University of Kaiserslautern, Kaiserslautern, Germany, in 1990.

From 1986 to 1998, he was with the German Aerospace Center (DLR), Cologne, Germany. From 1991 to 1992, he was on leave at the AT&T Bell Laboratories, Murray Hill, NJ, USA. In 1998, he joined the University of Kiel, Kiel, Germany, where he is currently a Full Professor of electrical and information engineering. He has been supervising over 50/200/25 bachelor's/master's/Ph.D. students and has authored or coauthored some 280 peer-reviewed journal and conference papers being cited more than 13 000 times, wrote two textbooks, and holds about 20 patents. His research interests are in the general area of communication theory and applied information theory with applications in wireless radio communications, optical wireless communications, molecular communications, underwater communications, and simultaneous wireless information and power transfer.

Dr. Hoeher has been a Fellow of the IEEE, for his contributions to decoding and detection that include reliability information, since 2014. He received the Hugo-Denkmeier-Award in 1990, the ITG Award in 2007, and several best paper awards. From 1999 to 2006, he served as an Associate Editor for the IEEE TRANSACTIONS ON COMMUNICATIONS.

